NASA Technical Paper 1964

December 1981

Experimental Study of Noise Reduction for an Unstiffened Cylindrical Model of an Airplane Fuselage

Conrad M. Willis
and Edward F. Daniels

NASA

NASA Technical Paper 1964

1981

Experimental Study of Noise Reduction for an Unstiffened Cylindrical Model of an Airplane Fuselage

Conrad M. Willis
and Edward F. Daniels
Langley Research Center
Hampton, Virginia

NASA
National Aeronautics
and Space Administration

Scientific and Technical Information Branch

SUMMARY

Noise-reduction measurements have been made for a simplified model of an airplane fuselage consisting of an unstiffened aluminum cylinder 0.5 m in diameter by 1.2 m long with a 1.6-mm-thick wall. Noise reduction was first measured with a reverberant-field pink-noise load on the cylinder exterior to obtain data for validation of an airplane interior-noise prediction method being developed under another program. Next, noise reduction was measured by using a propeller to provide a more realistic noise load on the cylinder. Structural resonance frequencies and acoustic reverberation times for the cylinder interior volume were also measured.

Comparison of data from the relatively simple test using reverberant-field noise with data from the more complex propeller-noise tests indicates some similarity in both the overall noise reduction and the spectral distribution. However, all of the test parameters investigated (propeller speed, blade pitch, and tip clearance) had some effect on the noise-reduction spectra. Thus, the amount of noise reduction achieved appears to be somewhat dependent upon the spectral and spatial characteristics of the flight conditions.

INTRODUCTION

Increasing concern about energy-efficient airplanes has renewed interest in propeller technology. Implementation of some of the new concepts in fuel-efficient propeller designs is expected to impose high noise loads on the fuselage (ref. 1) and will require increased acoustic treatment to achieve interior noise levels equal to those of current turbofan airplanes. Studies are being conducted to develop methods for predicting the interior noise levels of both conventional and high-speed propellers such as the high-speed turboprop. (See refs. 2, 3, and 4.) Reference 2 presents results from the first phase of a NASA funded analytical study of fuselage noise reduction that predicts noise reduction for the simplified case of unstiffened cylinders with reverberant-field noise loads.

The present paper presents results of noise-reduction measurements made in a reverberant field to validate the analytical method developed in reference 2 and goes on to compare noise-reduction measurements for reverberant fields with propeller-noise loadings in a anechoic environment.

Noise reduction was measured in a reverberant field by using a speaker to apply a pink-noise loading to the cylinder exterior. The cylinder was then tested in an anechoic room by using a propeller-noise loading to determine whether the noise-reduction data for the two loading conditions showed any similarity and to determine the trends of noise-reduction variation with changes in the propeller test parameters. Measured propeller noise levels were compared with levels predicted by analytical methods. The simplified fuselage model used for the tests was an aluminum cylinder 0.508 m in diameter. The propeller used in the anechoic-environment test was a two-blade model having a diameter of 0.762 m and was driven by a variable-speed electric motor. A 1.22-m-diameter air jet provided for simulation of forward velocities of up to 25 m/s.

Noise-reduction data for several combinations of the test parameters of propeller speed, tip clearance, and blade-pitch angle are presented. Information is also presented on cylinder resonance frequencies, damping, and propeller noise loads.

SYMBOLS

D	diameter, m
d	tip clearance between propeller and cylinder wall, m
F	rotational speed, rpm
h	distance from microphone to end of cylinder (see fig. 1(b)), m
J	advance ratio of propeller, $30V_\infty/R_pF$
L	length of cylinder interior, 1.193 m
m	mode index, number of longitudinal half-waves in cylinder wall
N	mode index, number of circumferential acoustic waves in cylinder interior
n	mode index, number of circumferential full-waves in cylinder wall
q	mode index, number of axial acoustic half-waves in cylinder interior
R	radius of cylinder interior, 0.252 m
R_p	radius of propeller, 0.381 m
r	radial location, m
s	mode index, radial acoustic waves in cylinder interior
T_R	time required for acoustic or structural vibration to decay 60 dB
V_∞	forward speed, m/s
x	microphone axial location, distance aft of propeller plane, m
β	angular location of propeller blade (see fig. 1(c)), deg
θ	propeller-blade pitch, deg
ϕ	angular location of microphone, measured from line on cylinder lying opposite the cylinder support structure (see fig. 1(b)), deg

Abbreviations:

CRT	cathode-ray tube
DVM	digital voltmeter
FFT	fast Fourier transform

OASPL overall sound pressure level

PSD power spectral density

SAE Society of Automotive Engineers

SPL sound pressure level

MODEL AND APPARATUS

The model was an unstiffened aluminum cylinder with closed ends 0.508 m in diameter and 1.245 m long. The test facilities were a reverberation room with a speaker for the noise source and an anechoic room with a propeller-noise source. Schematic diagrams of the test setups and some of the acoustic characteristics of the facilities are presented in figure 1. For the reverberant-field test (fig. 1(a)) the cylinder was supported by elastic cord. Cylinder interior noise levels were measured by a radial array of six microphones that was traversed axially and circumferentially to the desired measurement locations within the cylinder. Exterior noise levels were measured by using two microphones mounted at a distance of about 0.25 m from the cylinder wall. Pink noise was generated by a 100-watt speaker. Speaker location was adjusted to produce a uniform acoustic field near the model.

Schematic diagrams of the test setup for propeller-noise measurements in the anechoic room are presented in figures 1(b) and 1(c). Cylinder-interior noise measurements (fig. 1(b)) were made by using the microphone arrangement previously described for the reverberant-field tests, but the elastic-cord mounting was replaced by a rigid attachment. For measurements of noise levels on the model exterior surface (fig. 1(c)), the test cylinder was replaced by an equal-sized wood cylinder that had 10 microphones flush mounted on its surface. Separate models were used for interior and exterior measurements because of concern about the effect on the interior measurements of mounting holes for exterior microphones. Several sets of mounting holes were drilled in the support fixture to provide for changes in propeller tip clearance d by lateral translation of the cylinder and changes in the microphone-location coordinate x by longitudinal translation of the cylinder. Azimuthal location ϕ of the flush-mounted microphones was changed by rotating the cylinder.

The propeller blade was a 0.3-scale model of a Hartzell design for a Twin Otter airplane. Propeller diameter was 76.2 cm, and the maximum blade width was 5.3 cm. Blade pitch could be manually adjusted by rotating the blade in its mounting socket. A 43-kW variable-speed, water-cooled electric motor having a 0.23-m diameter was used to drive the propeller. The propeller was positioned on the center line and was 0.91 m downstream of the nozzle exit of a 1.22-m-diameter air duct used to simulate airplane forward velocity. An aerodynamic fairing representing the airplane nose was attached to the nozzle to prevent flow impingement on the flat end of the cylinder. A photograph of the test setup is presented in figure 2. Model details and microphone locations are shown in figure 3. The cylinder was formed from a sheet of 1.63-mm-thick aluminum and has an epoxy-bonded butt-joint seam with a 5-mm-wide exterior strap. Epoxy cement was also used to attach the cylinder end rings used to approximate shear diaphragm boundary conditions for the model structure. Six 6-mm-diameter condenser microphones were mounted on an adjustable radial bar. Modeling clay was pressed around the microphone cables to seal the access hole in the end of the cylinder.

A schematic diagram of the instrumentation used to acquire and reduce the data is presented in figure 4. High-pass filters were used to block low-frequency components from the microphone signals. For the reverberant-field tests (fig. 4(a)), a single-channel spectrum analyzer with a memory file was used to acquire and store a spectrum from an exterior microphone; the analyzer was then switched to an interior microphone and the difference in levels of the exterior and interior spectra was plotted to obtain noise reduction. For the more complex propeller-noise test (fig. 4(b)), most of the data-acquisition process was placed under the control of a 16-bit minicomputer to reduce test time and cost. Multiplexers stepped a digital voltmeter through all microphone channels and switched the channels specified at the computer keyboard to a one-third octave analyzer and a 500-line FFT digital-signal processor. The computer produced on-line plots of the data and also stored it for future use. A once-per-revolution pulse from a transducer on the propeller shaft was used to relate time histories of sound pressure level to propeller azimuth angle. A 14-channel magnetic tape recorder was used to store some of the data for post-test analysis.

TESTS

Reverberant Field

All tests were conducted with the speaker adjusted to produce about 110-dB OASPL on the cylinder exterior. At this exterior level all bands of the interior one-third octave spectrum were considered high enough for reasonable measurement accuracy. Internal microphone locations were selected to represent equal volumes by assuming longitudinal symmetry about the center and selecting five test stations equally spaced over one-half of the cylinder length. At each longitudinal station four azimuthal measurement locations were selected, starting at the cylinder seam. At each of the 20 locations, OASPL was recorded for all microphones and spectra were obtained for one exterior microphone and for the interior microphones at $r/R = 0.82$ and 0.55.

Propeller Noise

The ranges of test parameters investigated for the propeller-noise test were propeller speeds from 1000 to 4000 rpm, propeller-blade pitch settings of 10° and 20°, propeller locations having tip clearances (distance from propeller disk to the fuselage) of 0.2, 0.3, and 0.4 of the propeller tip radius, and forward velocities from 0 to 20 m/s. These values were intended to cover partially the range of parameters applicable to general aviation aircraft. The method of operation during testing was to start the flow in the forward velocity nozzle, start the propeller, and then store the data at each selected rotational speed in the computer files. Noise-reduction spectra were obtained by subtracting interior spectra acquired by using the aluminum cylinder from computer-stored exterior spectra acquired by using the wood cylinder during a previous run at the same rotational speed, blade pitch, and tip clearance.

RESULTS AND DISCUSSION

Measurements of sound pressure levels inside an unstiffened, closed aluminum cylinder were subtracted from exterior measurements to obtain noise-reduction data for the cylinder with two types of exterior noise, a reverberant field and propeller

noise. The reverberant-field data are presented in figures 5 to 7 and are compared with theory in figure 8. Propeller-noise data are presented in figures 9 to 12, and noise reduction for propeller noise is compared with that for reverberant-field pink noise in figure 13. Some information on the structural and acoustic properties of the cylinder is presented in appendix A, and characteristics of propeller noise are presented in appendix B.

Noise Reduction in a Reverberant Field

Spatial variation of noise reduction.- The longitudinal variation in overall noise reduction is presented in figure 5(a) for a radial location of $r/R = 0.82$. There was essentially no variation along the length of the cylinder; all six measurement locations had values within ±0.3 dB of the average. Radially (fig. 5(b)), the noise reduction varied smoothly from about 18 dB near the center to about 13 dB at $r/R = 0.82$. Variation of noise reduction in the circumferential direction was not considered significant; however, data at $\phi = 180°$, or along the cylinder radius that passes through the cylinder seam, were slightly lower than the noise reduction measured at other circumferential locations.

Noise-reduction spectra.- One-third octave-band noise-reduction spectra were obtained for each interior-measurement location by subtracting the level of each interior band from the corresponding exterior measurement. A typical set of spectra is shown in figure 6. From 50 to 5000 Hz the exterior spectrum was fairly flat and was a reasonably good representation of the nominal pink-noise distribution. Below 50 Hz the exterior acoustic field becomes less diffuse and accurate measurement of the exterior level is more difficult. The interior response is highest in the range from 1000 to 3000 Hz and has peaks in the 125- and 160-Hz bands and another peak at the 250-Hz band. These three bands contain the first five structural modes of the cylinder. (See appendix A.) Reference 2 presents the interior-response data, estimates damping, and identifies the modal pairs of coupled acoustic and structural modes making a major contribution to the sound pressure level of each band. This analysis attributes the peak in the 125- and 160-Hz bands mainly to structural modes at 132 and 160 Hz which are coupled, respectively, to acoustic modes having frequencies of 1143 and 903 Hz. (See appendix A.)

Noise-reduction spectra for three radial locations are presented in figure 7. Minimum noise reduction occurred in the range from 1000 to 3000 Hz, and the maximum spread of data for the three locations was about 28 dB at 250 Hz. Noise reduction was about the same for all radial locations at the 125- and 160-Hz bands and above 3000 Hz; for the remainder of the spectrum, noise reduction generally increased with distance from the cylinder wall.

Comparison of predicted and measured SPL.- Predicted and measured noise reductions are compared in figure 8. The measured spectrum was calculated from the average squared sound pressure over one-half of the cylinder volume. The predicted noise-reduction spectrum is from reference 2 which calculates noise reduction by using measured or estimated damping coefficients and resonance frequencies as part of the input. (See appendix A.) The predicted noise reduction is considered to show rather good agreement with measured data throughout the range presented from 50 to 5000 Hz. Frequencies below 50 Hz are considered of minor importance because they are below the lowest structural resonance, and scaling the cylinder to airplane size would extend the data well below the blade-passage frequency range for the most general aviation aircraft.

Noise Reduction with Propeller-Noise Loadings

Exterior and interior sound pressure levels were measured at several propeller operating conditions. A model of a propeller used on a general aviation twin-engine airplane was tested at speeds providing blade-passage frequencies representative of flight conditions; therefore, the data are considered realistic enough to be used for comparison with the reverberant-field data and to indicate the trends of the various test parameters.

All of the propeller-noise data presented are for $\phi = 0°$, the cylinder element nearest the propeller disk, because the forward-speed nozzle flow only partially enveloped the cylinder. (See fig. 1(a).) All noise-reduction spectra presented are for $r/R = 0.82$, the microphone location nearest the cylinder wall.

Exterior and interior OASPL.- Overall sound pressure levels for the exterior and interior of the cylinder are presented in figure 9. Longitudinal variation in the exterior OASPL was about 10 dB over the range of measurement locations of -0.7 to 1.2 propeller radii aft of the propeller plane. The OASPL at the propeller plane were about 3 dB below the maximum levels occurring a short distance forward and aft of the propeller plane. Additional information on the characteristics of the propeller exterior noise is given in appendix B. Interior levels were about 20 to 30 dB below the exterior levels.

Effect of tip clearance on noise reduction.- Noise reduction for two values of tip clearance is presented in figure 10. Increasing clearance from 0.2 to 0.3 propeller radii increased noise reduction by about 12 dB from 200 to 400 Hz and provided smaller increases over most of the remainder of the spectra. Spectrum shape was generally similar, but the minimum noise reduction, 7 dB for both conditions, was two-thirds octave lower in frequency for the larger tip clearance.

Effect of blade pitch on noise reduction.- Noise-reduction spectra for propeller-blade pitch angles of 10° and 20° are presented in figure 11. The 10° blade pitch provided more noise reduction, up to 18 dB higher, in the range from 200 to 500 Hz. Over the remainder of the spectrum, pitch had little effect on noise reduction.

Effect of propeller speed on noise reduction.- Noise-reduction spectra for 2000 and 4000 rpm are presented in figure 12. The frequencies of some of the blade-passage harmonics are indicated at the top of the figure. The peaks in the noise-reduction spectra tend to occur in the bands containing blade-passage harmonics. No other trend was obvious, and the 2000-rpm spectra were above the 4000-rpm spectra for about one-half of the analysis bands. Overall noise reduction was 21 dB for the 4000-rpm condition at 20° and was about 9 dB higher for the other three conditions.

Comparison of noise reduction for propeller noise and reverberant field.- Figure 13 presents a comparison of noise reduction for reverberant-field and propeller-noise loads on the cylinder exterior. Variation of overall noise reduction with radial location (fig. 13(a)) is similar for the two conditions, but the level is somewhat higher for propeller noise. Spectral variation (fig. 13(b)) is also similar; each spectrum has a peak near 100 Hz and falls off to a minimum near 1600 Hz, and the reverberant-field levels fall near or within the range of the propeller data for nearly one-half of the analysis bands. One notable difference occurs at the 125- and 160-Hz bands. The higher noise reduction measured for propeller noise in these two bands may result from the lower exterior levels at high frequencies (see

appendix B) exciting less interior response in the cylinder at the 1143- and 903-Hz acoustic modes that are coupled to the structural modes (m,n = 1,4 and 1,3) resonant in the 125- and 160-Hz bands, respectively. (See appendix A.)

In general, noise reduction for the simplified model fuselage tested varied with the spectral distribution of the exterior load, but some similarities do exist between noise-reduction results for the reverberant-field and propeller-noise exterior loading conditions.

CONCLUDING REMARKS

Noise-reduction measurements have been made for a simplified model of an airplane fuselage consisting of an unstiffened aluminum cylinder. Tests were conducted in two noise environments, reverberant-field pink noise and propeller noise in an anechoic room.

Measured noise reduction for the model in a reverberant field agreed well with predicted noise reduction from reference 2, thus validating the prediction method.

Comparison of results for the two noise-loading conditions shows some similarity in the noise-reduction spectra. However, all of the test parameters investigated had at least a minor effect on noise reduction, and, thus, the accuracy of the results appears to be somewhat dependent upon the fidelity with which the exterior noise represents the desired flight condition.

Langley Research Center
National Aeronautics and Space Administration
Hampton, VA 23665
November 23, 1981

APPENDIX A

RESONANCE FREQUENCIES AND DAMPING

Frequencies of the structural vibration modes of the test cylinder were calculated as an aid in the interpretation of the noise-reduction data presented in the main text of this paper. This appendix also lists the cylinder acoustic modes calculated in reference 2 and some measurements of the acoustic and structural reverberation times made for use in estimating damping coefficients.

For this phase of the testing the cylinder was removed from the reverberation room and was suspended by elastic cord. A schematic diagram of instrumentation for the reverberation-time measurements is presented in figure 14. A 15-cm-diameter speaker was mounted a few centimeters from the cylinder wall, on the inside for some test points and on the outside for the others. Microphones were mounted near the cylinder wall, and lightweight accelerometers were mounted on the wall. The decay rate for the acoustic or structural vibration after termination of excitation by the speaker was determined by passing the microphone and accelerometer signals through a one-third-octave filter and logarithmic voltage converter to a plotter. A time history of instantaneous voltage of the transducer signal was also recorded. A few of the structural-vibration modes were identified by driving the speaker with a tone, varying the frequency to tune a resonance, reading the frequency from a meter, and determining the mode indices by sweeping a hand-held microphone past the cylinder and counting the phase changes indicated by rotations of a CRT Lissajous display.

The predicted mode lattices for structural and acoustic modes of cylinder vibration are presented in figure 15 in order of increasing frequency. The structural modes, which were calculated from well-known formulas for thin, circular, cylindrical shells given in chapter 2 of reference 5, are listed as follows:

$$f_{m,n} = (\Omega/2\pi R)\{E/[\rho(1 - \mu^2)]\}^{1/2}$$

where

$$\Omega = \left[\frac{(1 - \mu^2)\lambda^4}{(n^2 + \lambda^2)^2} + k(n^2 + \lambda^2)^2\right]^{1/2}$$

$$\lambda = m\pi R/L$$

$$k = t^2/12R^2$$

The undefined symbols and values assigned for this calculation are as follows:

E Young's modulus, 6.89×10^{10}, Pa

t cylinder-wall thickness, 0.00163 m

μ Poisson's ratio, 0.3

ρ density of structural material, 2710 kg/m^3

APPENDIX A

The free-free inextensional cylinder mode (Rayleigh) bounding the mode lattice was calculated by

$$f_F = (\Omega_F/2\pi R)\{E/[\rho(1 - \mu^2)]\}^{1/2}$$

where

$$\Omega_F = [kn^2(n^2 - 1)^2/(n^2 + 1)]^{1/2}$$

The ring frequency was calculated to be 3312 Hz by

$$f_R = (1/2\pi R)\{E/[\rho(1 - \mu^2)]\}^{1/2}$$

and the coincidence frequency was calculated to be 7892 Hz by

$$f_c = (c^2/2\pi)(12\rho/Et^2)^{1/2}$$

where c is the acoustic velocity in air, assumed to be 343 m/s. The frequencies of a few modes measured to check the calculations agreed within about ±1 percent. Acoustic modes from reference 2 are presented in figure 15(b).

Some sample time histories of the decay of an acoustic vibration inside the cylinder are presented in figure 16. Decay of the acoustic mode excited by a 400-Hz tone, shown at the top of figure 16, was very smooth and regular and the data were reduced by using a log converter. (See fig. 14.) One-third octave-band excitation tended to produce acoustic fields that appeared to have a beat of two or more modes in the decay as shown for the 1000-Hz band record in the center of figure 16. This type of data was manually reduced by plotting the amplitude represented by the separation of the hand-faired boundary lines. At some excitation frequencies coupling with modes at other frequencies was strong and decay was irregular, even with tone excitation as shown in the 250-Hz band record at the bottom of figure 16. Some of the reverberation times obtained from the decay time histories are presented in figure 17. These reverberation times were provided to the authors of reference 2 for use in estimating damping coefficients required as input to their prediction program for interior noise.

APPENDIX B

PROPELLER-NOISE LOADS ON CYLINDER

After completing noise-reduction tests of the cylindrical fuselage model in a reverberant-field environment, additional measurements were made with propeller noise in an anechoic room to obtain data for comparison with the simpler tests. The data are presented in this appendix to show some of the characteristics of propeller-noise loading on an airplane fuselage sidewall.

Test-facility capabilities and the simplified fuselage model used placed some limitations on the range of test parameters and on the realism of flight simulation. Therefore, some of the measured loads were compared with loads calculated by analytical and empirical prediction programs (refs. 6 and 7) that were considered representative of flight conditions. This comparison is presented in figure 18. The prediction methods calculate the free-field noise levels, and no correction was made for the increase in level due to the presence of the fuselage; therefore, the calculated values would be expected to be a few decibels lower than measured levels. The Farassat program (ref. 6) utilizes linear solutions to the Ffowcs Williams-Hawkins equation, whereas the SAE method is mainly empirical and probably not as accurate for configurations not included in the SAE data base of reference 7. Most of the measured levels were a few decibels above the calculated loads as expected, and the trends of the measured variation were similar to the Farassat predictions for both the longitudinal variation of OASPL (fig. 18(a)) and the variation of harmonic level (fig. 18(b)). There is a slight dip in OASPL at the propeller plane, and the maximum noise level occurred about 0.2 propeller radii aft of the propeller plane. Harmonic level decreased about 3 dB per harmonic. All of the propeller data presented are for $\phi = 0°$, the cylinder element nearest the propeller disk, because this location was farther inside the flow from the forward-speed nozzle.

A propeller-synchronized, averaged time history of the variation in sound pressure level due to blade passage is presented in figure 19. The data shown are the average instantaneous SPL for 64 two-revolution periods, each starting at $\beta = -12°$. Sound pressure levels of random phase or temporal distribution tend to cancel each other after a sufficient number of averages while retaining all pressures that are synchronous with the propeller. Near the propeller plane (fig. 19(a)), the maximum pressure peaks are sharp with most of the buildup and decay occurring within a 25° interval of propeller rotation. Peak-to-valley amplitude of the blade-passage pressure was about 15 Pa at $x/R_p = -0.07$ and decreased with distance from the propeller plane to about 10 Pa at $x/R_p = -0.67$. (See fig. 19(b).) At the $x/R_p = -0.67$ location, the change in SPL appeared sinusoidal with the buildup and decay distributed over the entire 180° between successive blade passages. Peak pressures at the two locations appear to be inphase and occur slightly later than the closest approach of the propeller ($\beta = 0°$). Power spectral density for the blade-passage time history of figure 19(a) is compared with that for the total noise in figure 20. Harmonics of the blade-passage frequency are easily identified in the total noise spectrum up to about the eighth harmonic, and the harmonics are responsible for almost all the noise up to this frequency. At frequencies above the eighth harmonic (533 Hz), the blade-passage noise falls off and the PSD levels of the total noise spectrum are mainly due to the random noise.

Relative contributions of the blade-passage harmonics and random portions of the noise are again compared in figure 21 by using narrow-analysis bandwidth to allow

better measurement of the levels at frequencies between the harmonics. The first blade-passage harmonic is about 30 dB above the random noise which has approximately a white-noise distribution over the frequency range from 50 to 1000 Hz.

The effects of airplane forward velocity and propeller speed on OASPL are presented in figure 22. Low forward velocities (10 to 20 m/s) reduced the OASPL on the fuselage by about 8 dB. Noise level increased with propeller rotational speed, with about a 29-dB change between 1000 and 4000 rpm.

The effect of propeller tip clearance on overall sound pressure level is presented in figure 23. Doubling tip clearance produced a decrease of about 6 dB near the propeller plane and a decrease of about 3 dB at $\pm x/R_p = 0.6$.

REFERENCES

1. Hanson, Donald B.: Near Field Noise of High Tip Speed Propellers in Forward Flight. AIAA Paper No. 76-565, July 1976.

2. Pope, L. D.; Rennison, D. C.; and Wilby, E. G.: Analytical Prediction of the Interior Noise for Cylindrical Models of Aircraft Fuselages for Prescribed Exterior Noise Fields. Phase I: Development and Validation of Preliminary Analytical Models. NASA CR-159363, 1980.

3. Mixson, John S.; Barton, C. Kearney; and Vaicaitis, Rimas: Investigation of Interior Noise in a Twin-Engine Light Aircraft. J. Aircr., vol. 15, no. 4, Apr. 1978, pp. 227-233.

4. Dugan, James F.; Miller, Brent A.; Graber, Edwin J.; and Sagerser, David A.: The NASA High-Speed Turboprop Program. NASA TM-81561, [1980].

5. Leissa, Arthur W.: Vibration of Shells. NASA SP-288, 1973.

6. Martin, R. M.; and Farassat, F.: Users' Manual for a Computer Program To Calculate Discrete Frequency Noise of Conventional and Advanced Propellers. NASA TM-83135, 1981.

7. Prediction Procedure for Near-Field and Far-Field Propeller Noise. AIR 1407, Soc. Automat. Eng., Inc., May 1977.

Reverberation room

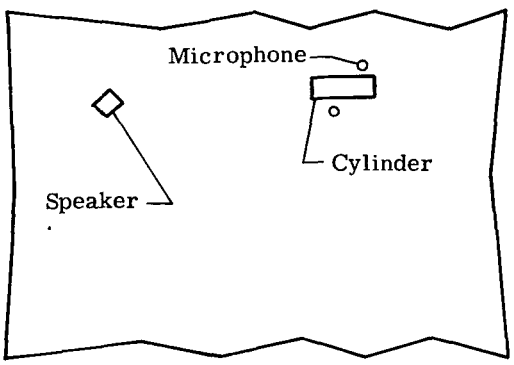

Splayed walls, 6 × 9 × 4 m;
range, 50 to 20 000 Hz;
reverberation time, 8 sec

Anechoic room

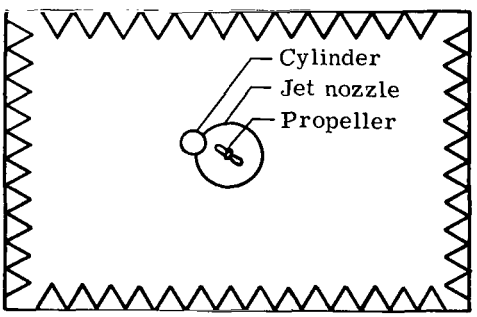

Size, 6 × 9 × 12 m;
range, 80 to 30 000 Hz;
absorption coefficient, 0.995

(a) Test facilities.

Figure 1.- Schematic diagrams of test facilities and apparatus.

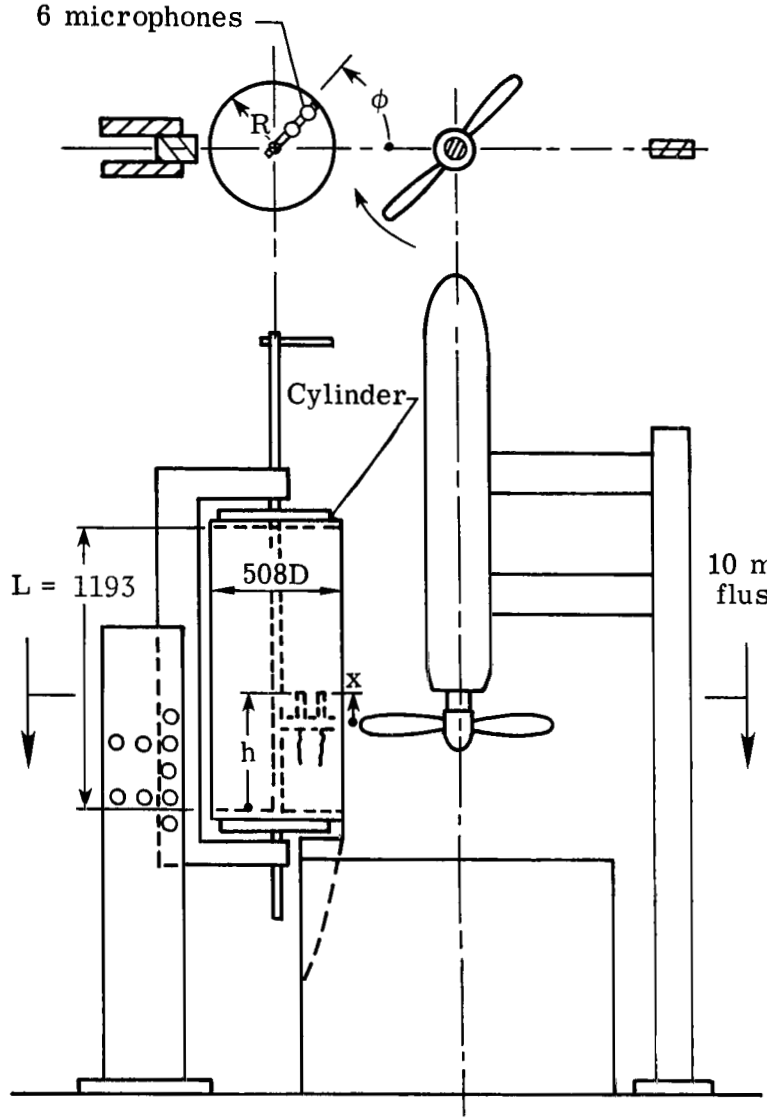

(b) Interior SPL measurement on aluminum cylinder.

Dimensions are given in mm.

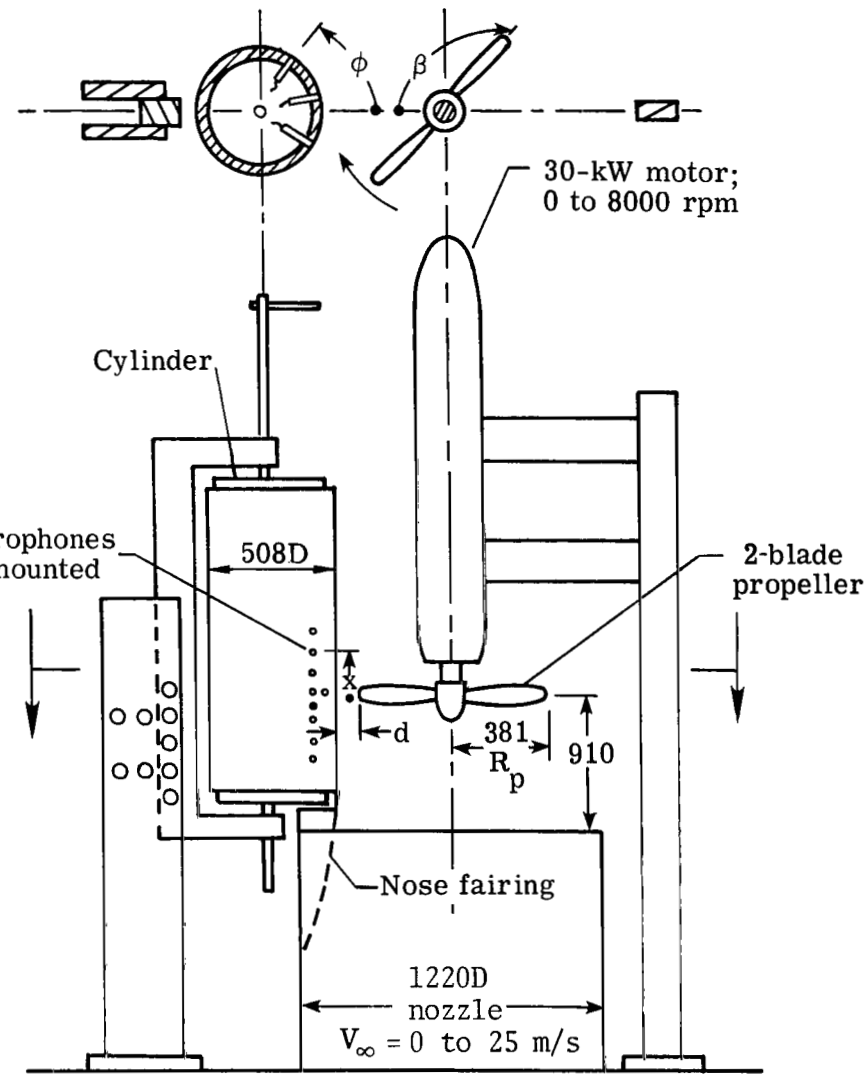

(c) Exterior SPL measurement on wood cylinder.

Dimensions are given in mm.

Figure 1.- Concluded.

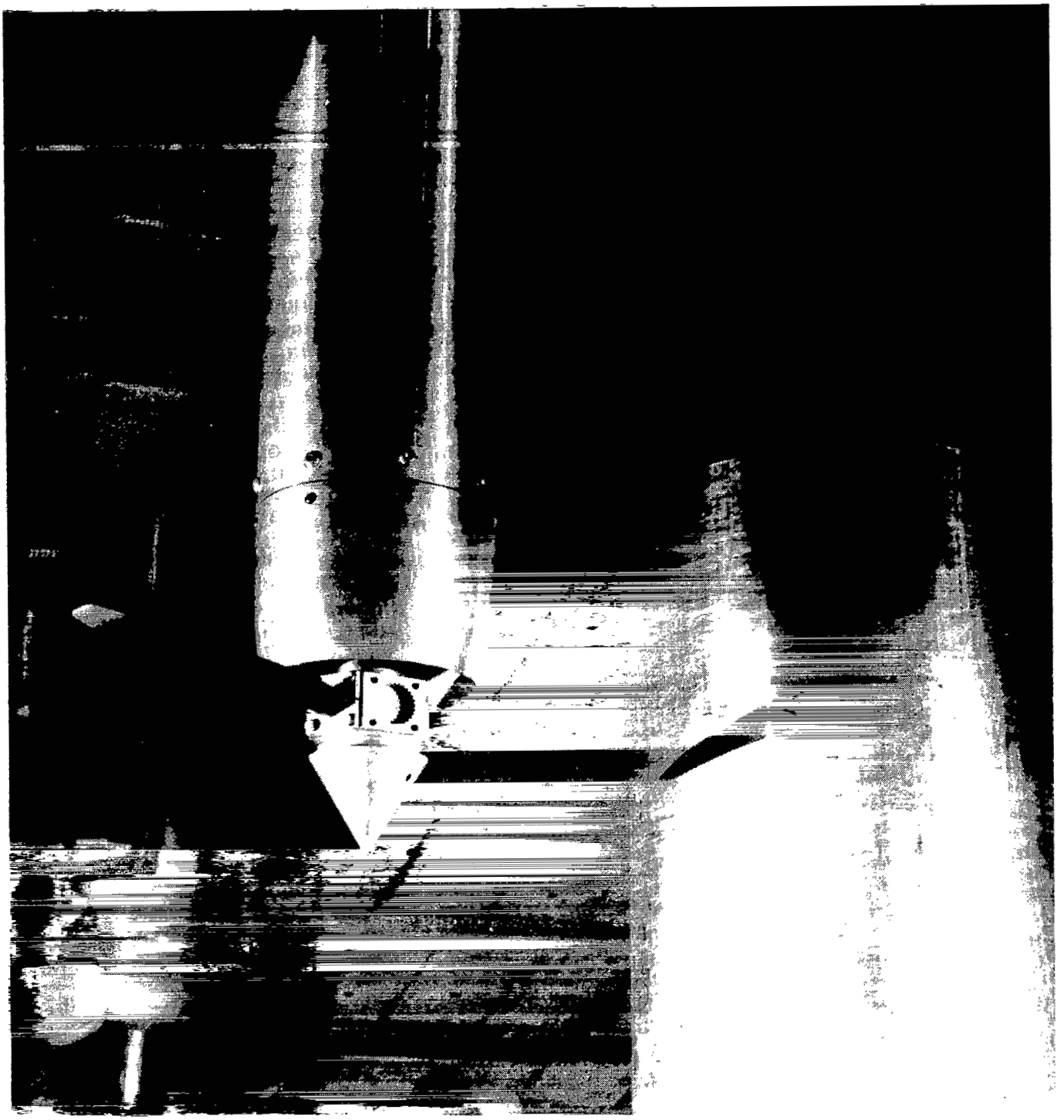

L-80-4964

Figure 2.- Photograph of test setup.

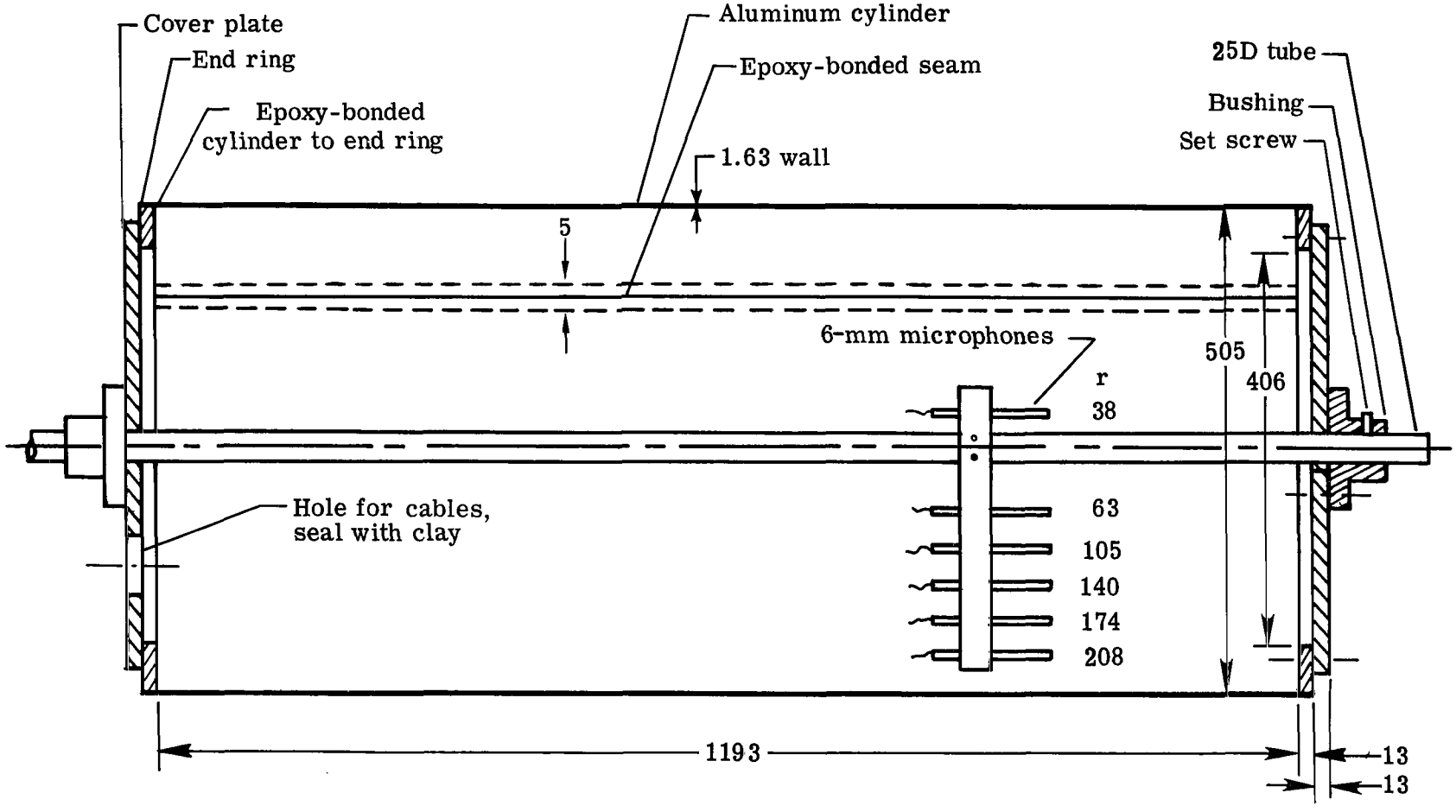

Figure 3.- Model details and microphone locations. Dimensions are given in millimeters.

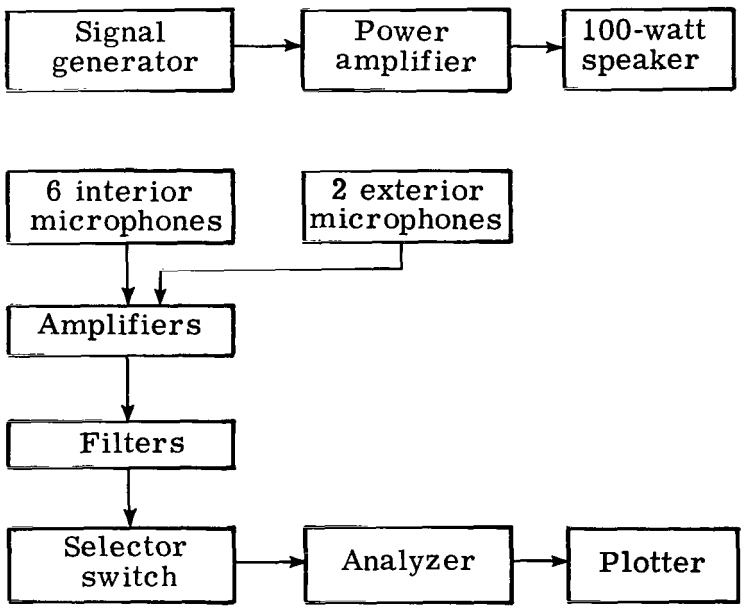

(a) Noise-reduction measurement with reverberant-field noise load on cylinder.

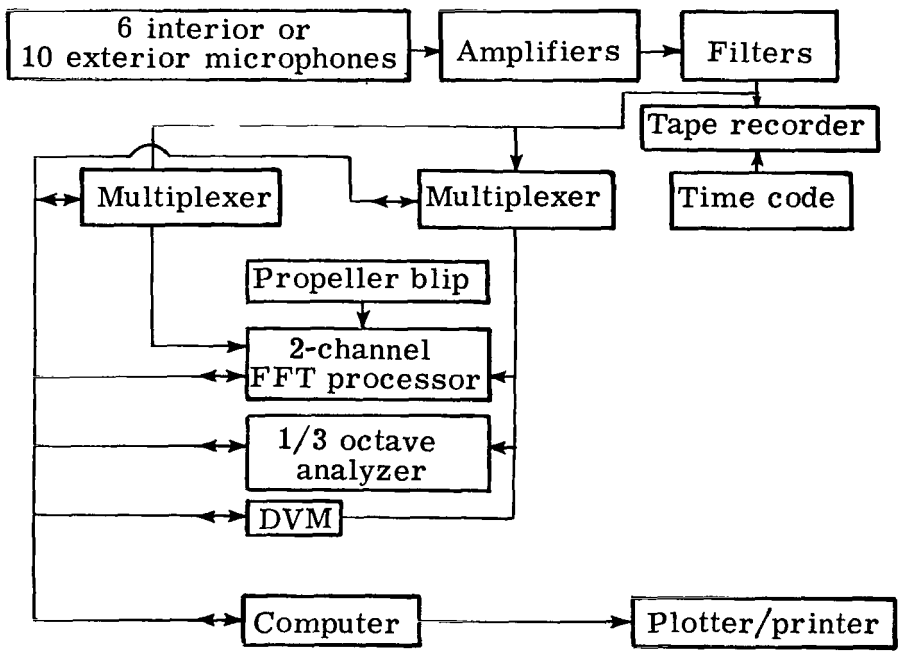

(b) Noise-reduction measurement with propeller noise.

Figure 4.- Schematic diagram of instrumentation.

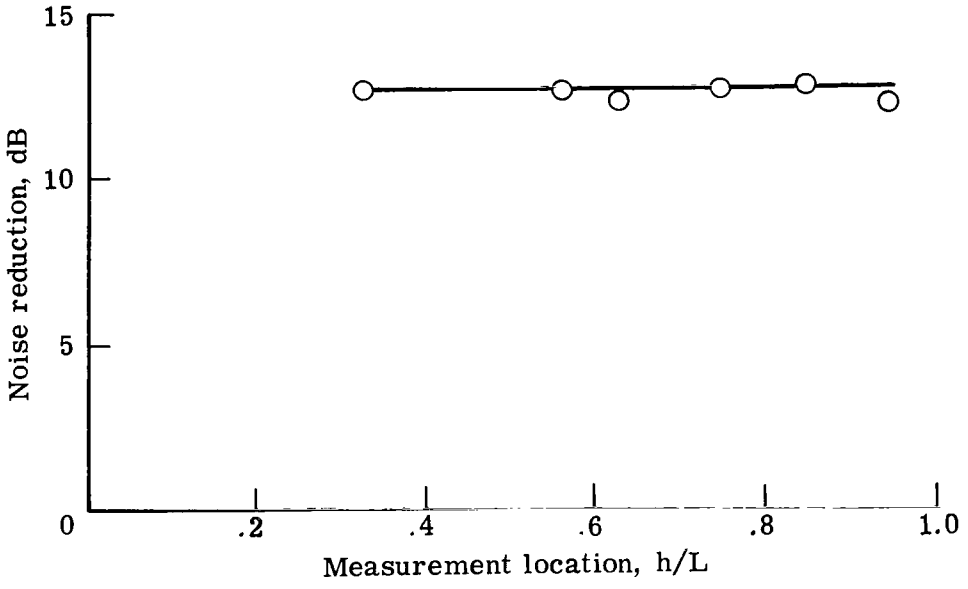

(a) Longitudinal variation. r/R = 0.82.

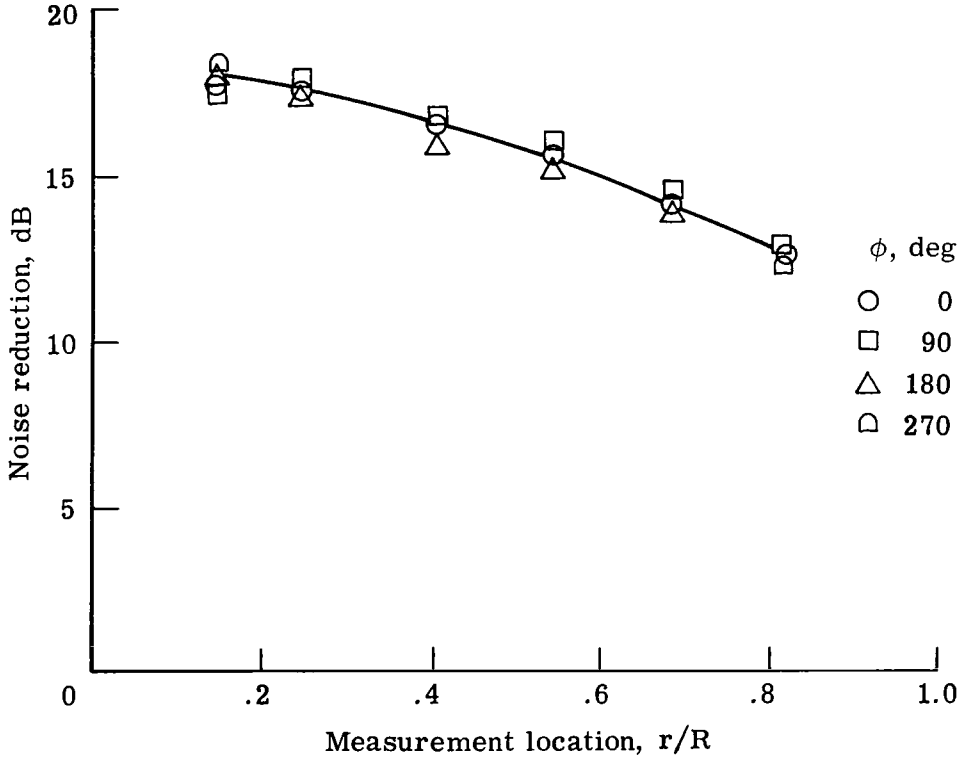

(b) Radial variation.

Figure 5.- Noise reduction for cylinder in reverberant field.

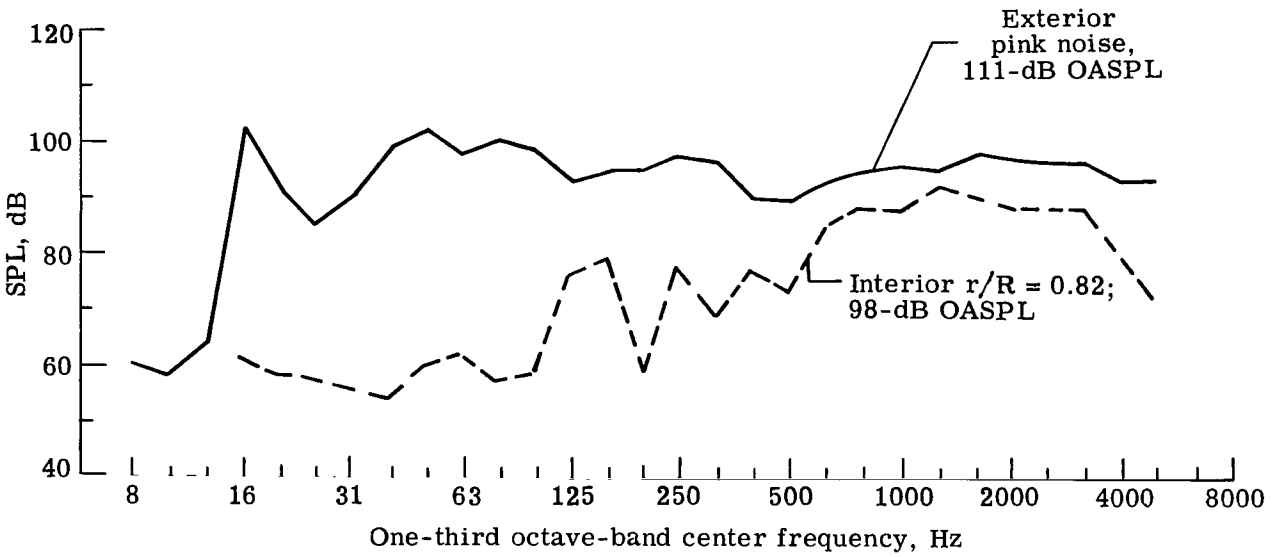

Figure 6.- Comparison of exterior and interior noise spectra for cylinder.

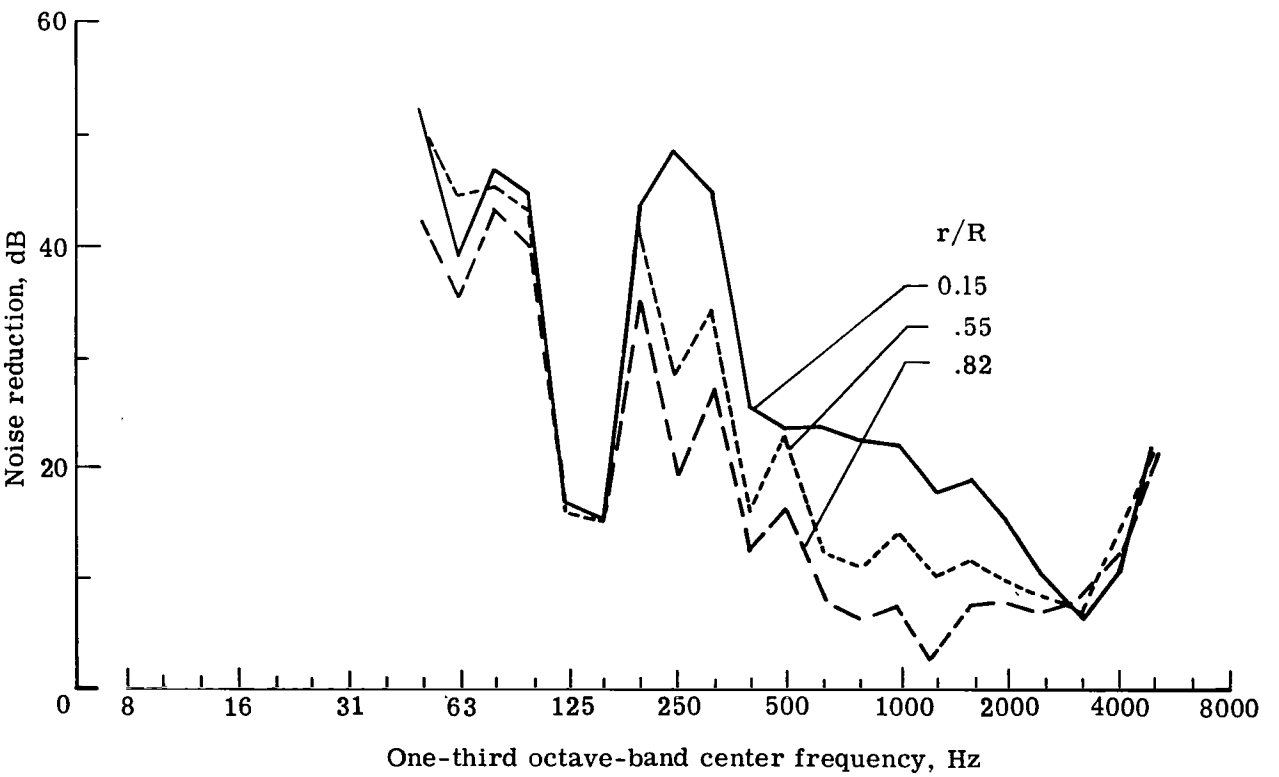

Figure 7.- Comparison of noise-reduction spectra at three radial locations.

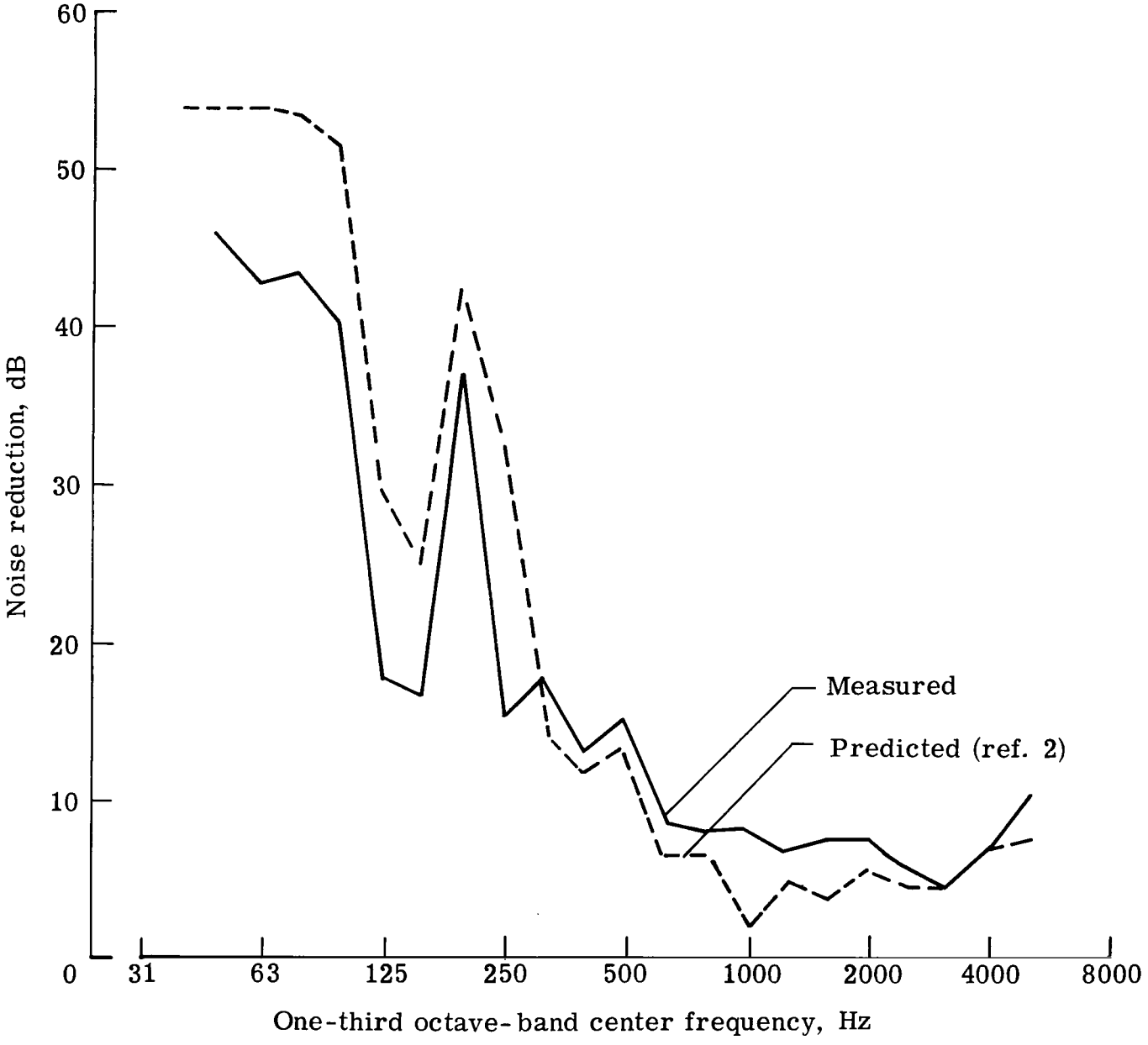

Figure 8.- Comparison of measured and predicted space-averaged noise-reduction spectra for cylinder in a pink-noise reverberant field.

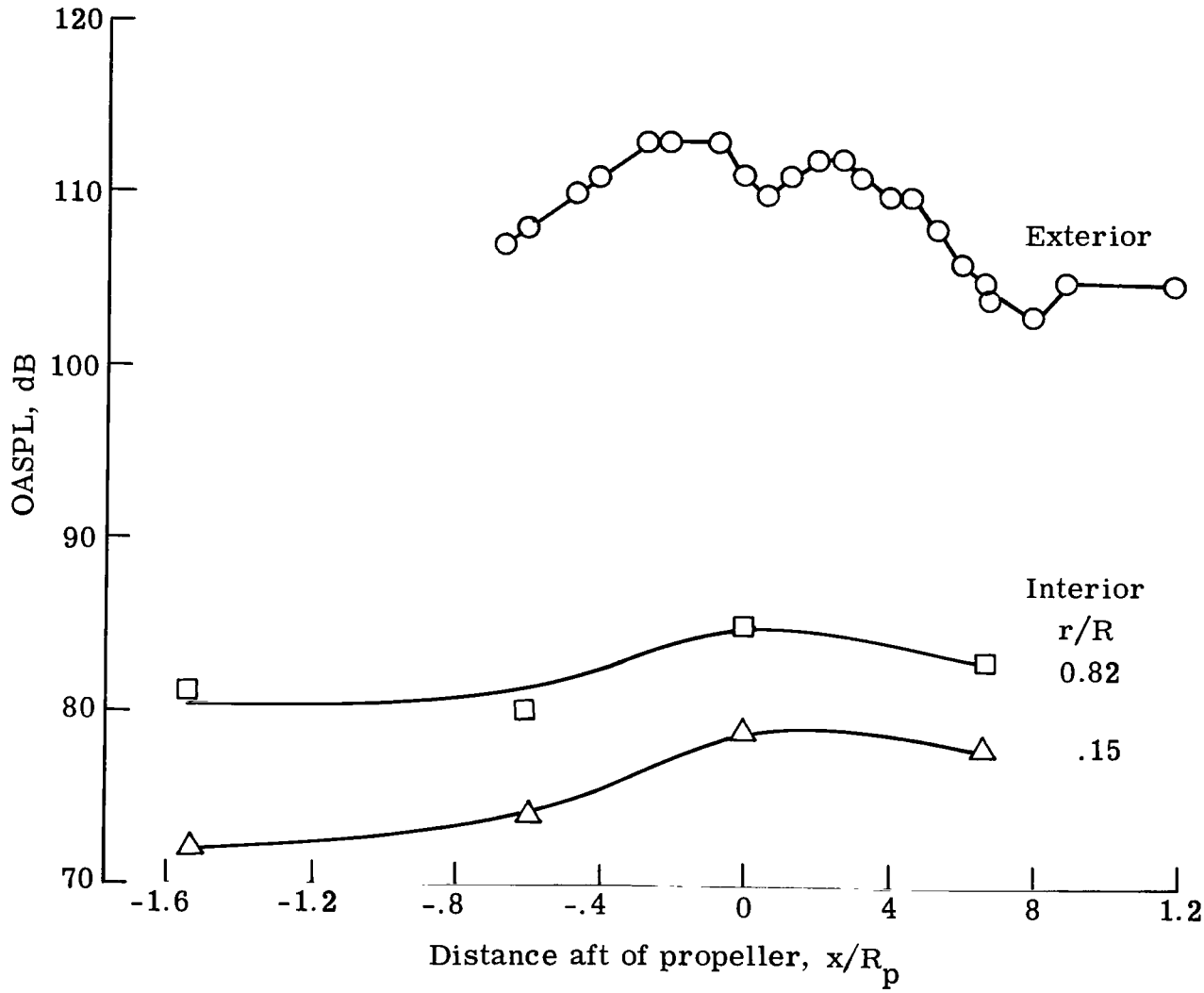

Figure 9.- Variation in exterior and interior OASPL along cylinder with propeller noise. 2000 rpm; V_∞ = 20 m/s; θ = 20°; d/R_p = 0.2.

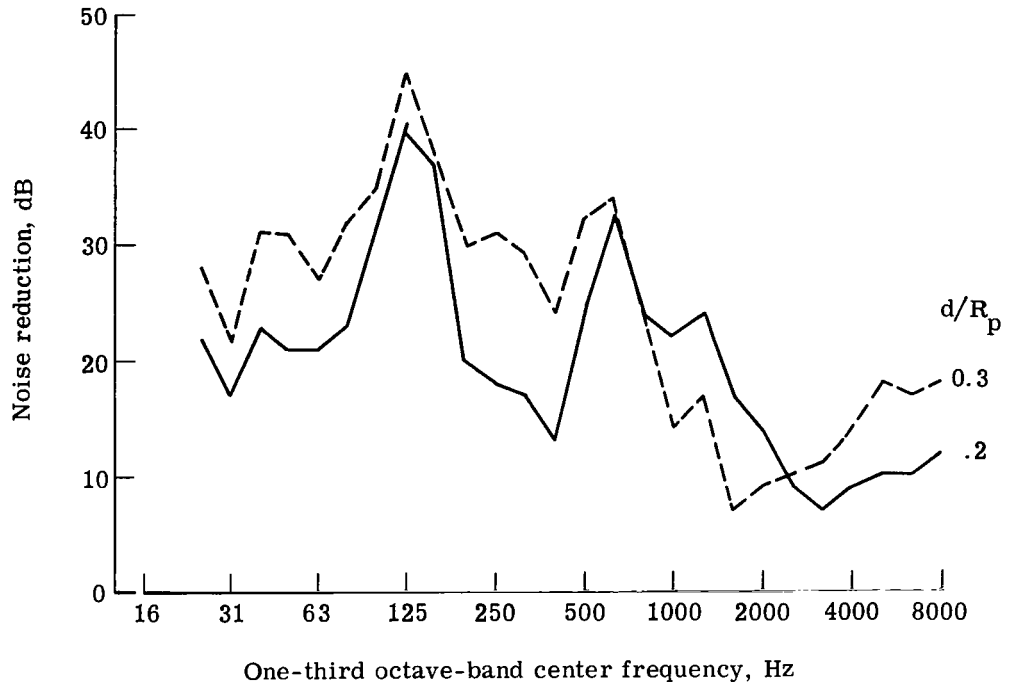

Figure 10.- Effect of propeller tip clearance on noise reduction. 4000 rpm; $\theta = 20°$.

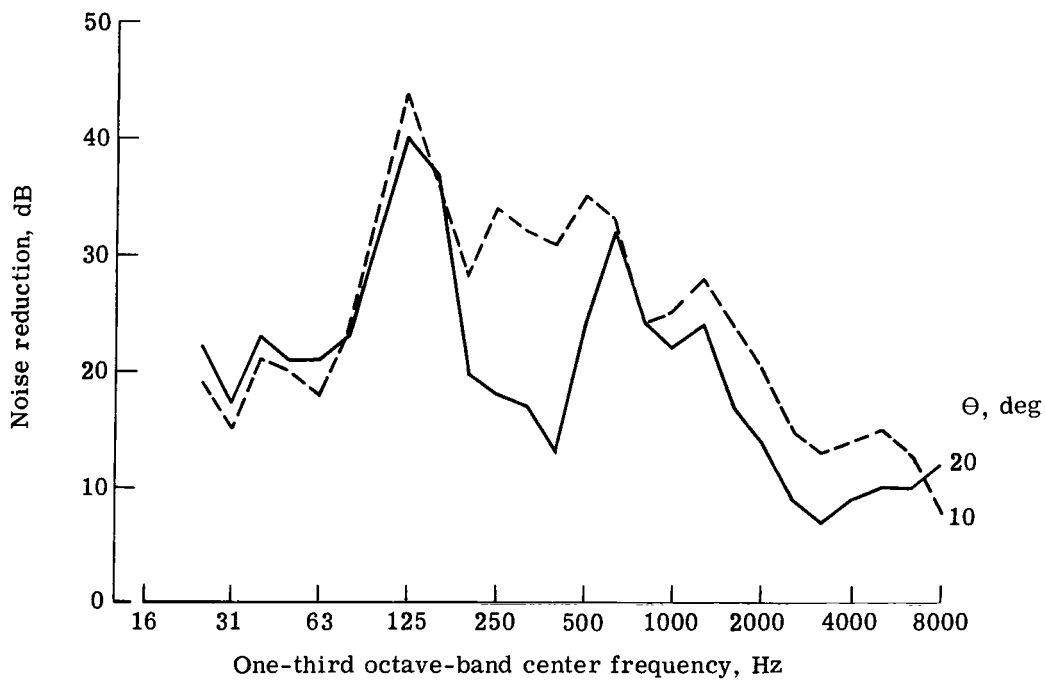

Figure 11.- Effect of propeller-blade pitch on noise reduction. 4000 rpm; $d/R_p = 0.2$.

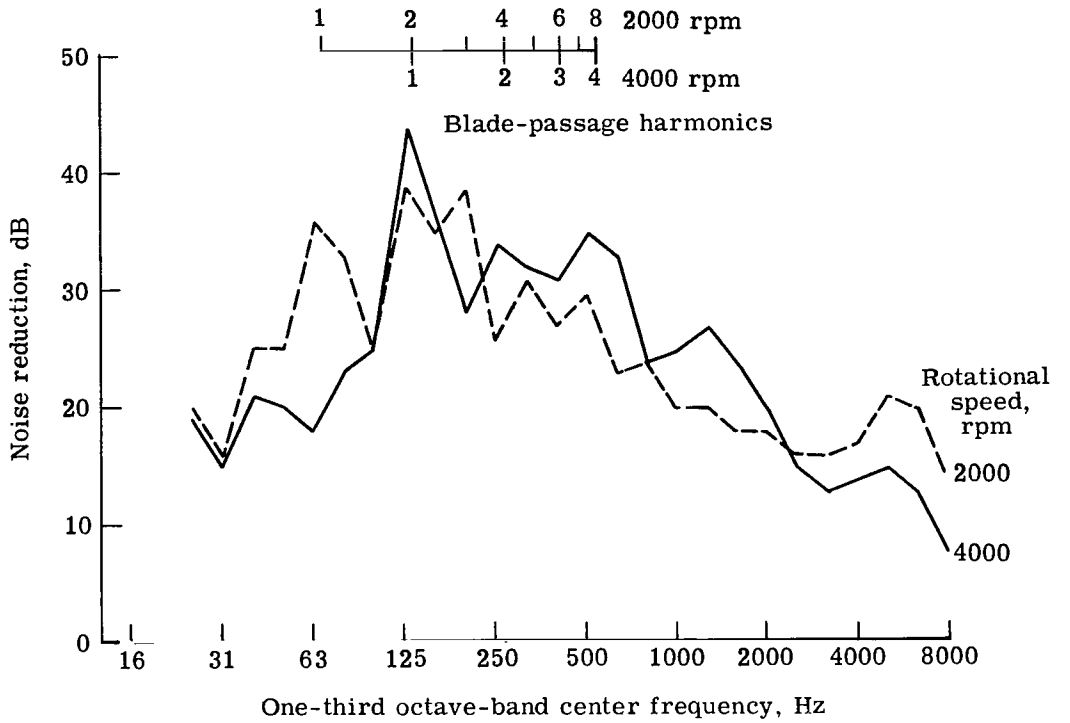

(a) Blade pitch, 10°.

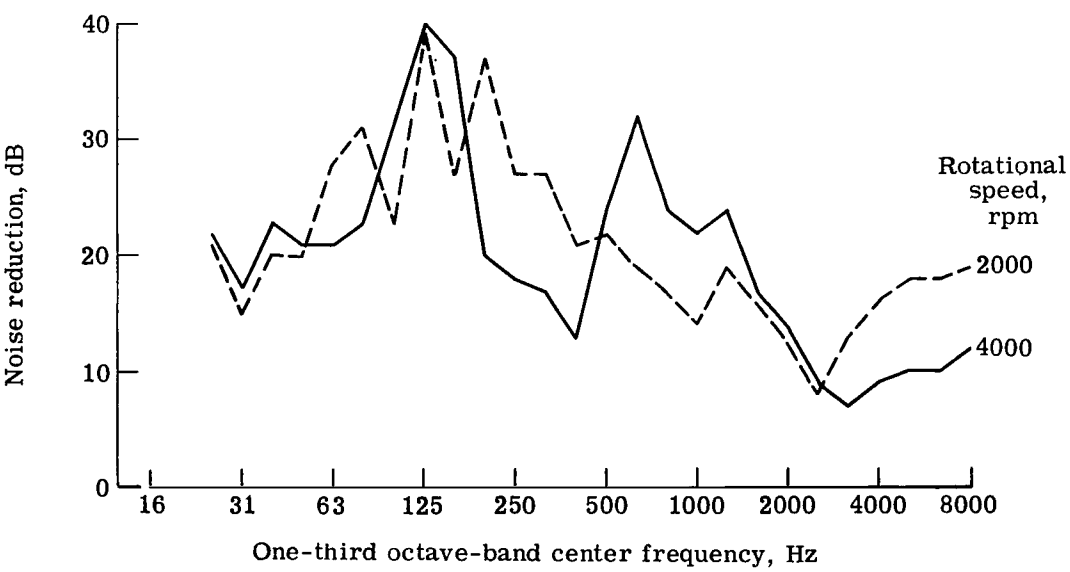

(b) Blade pitch, 20°.

Figure 12.- Effect of propeller speed on noise reduction. $d/R_p = 0.2$.

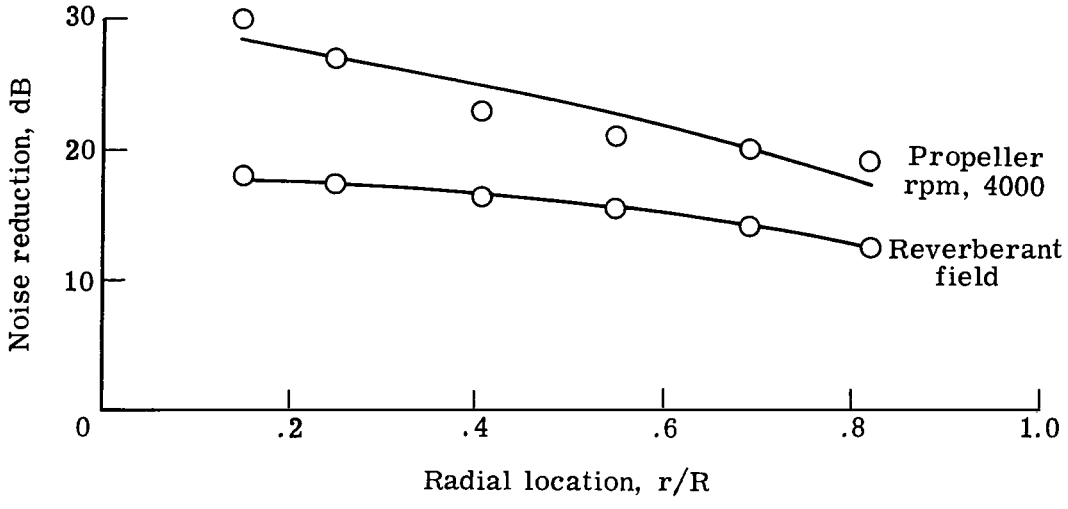

(a) Radial variation of overall noise reduction.

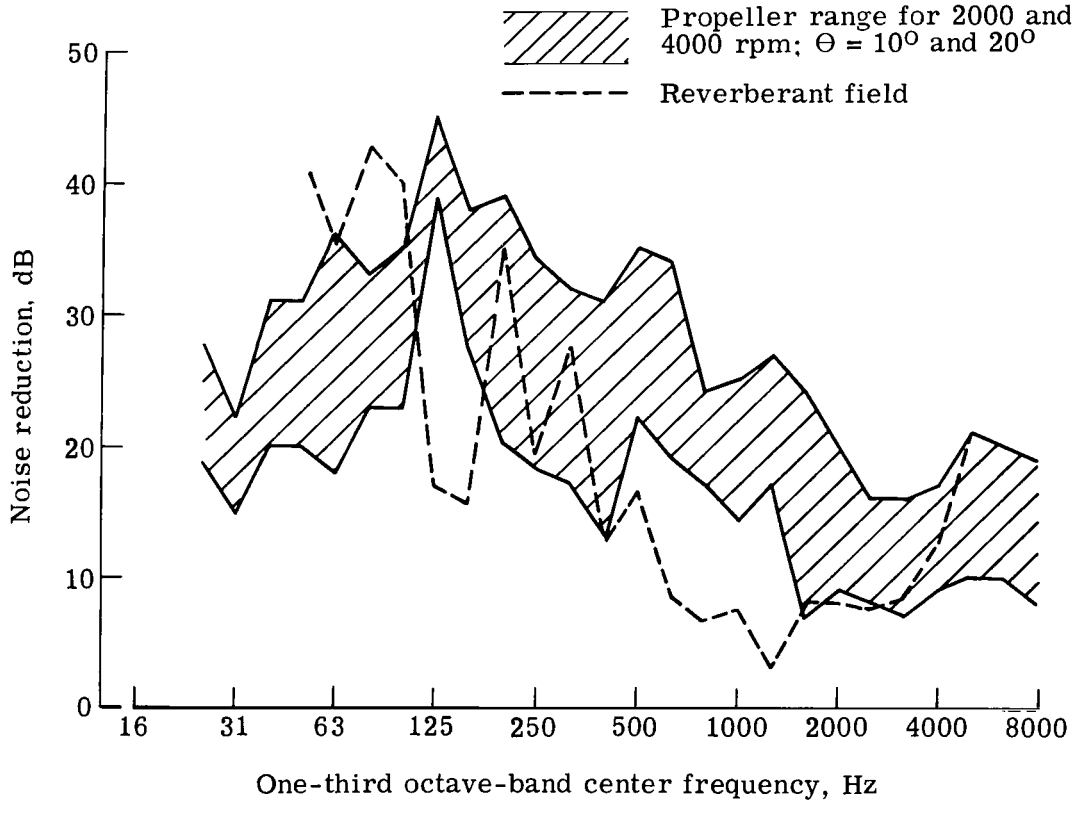

(b) Spectral comparison.

Figure 13.- Comparison of noise reduction for propeller noise and reverberant-field loads on cylinder exterior.

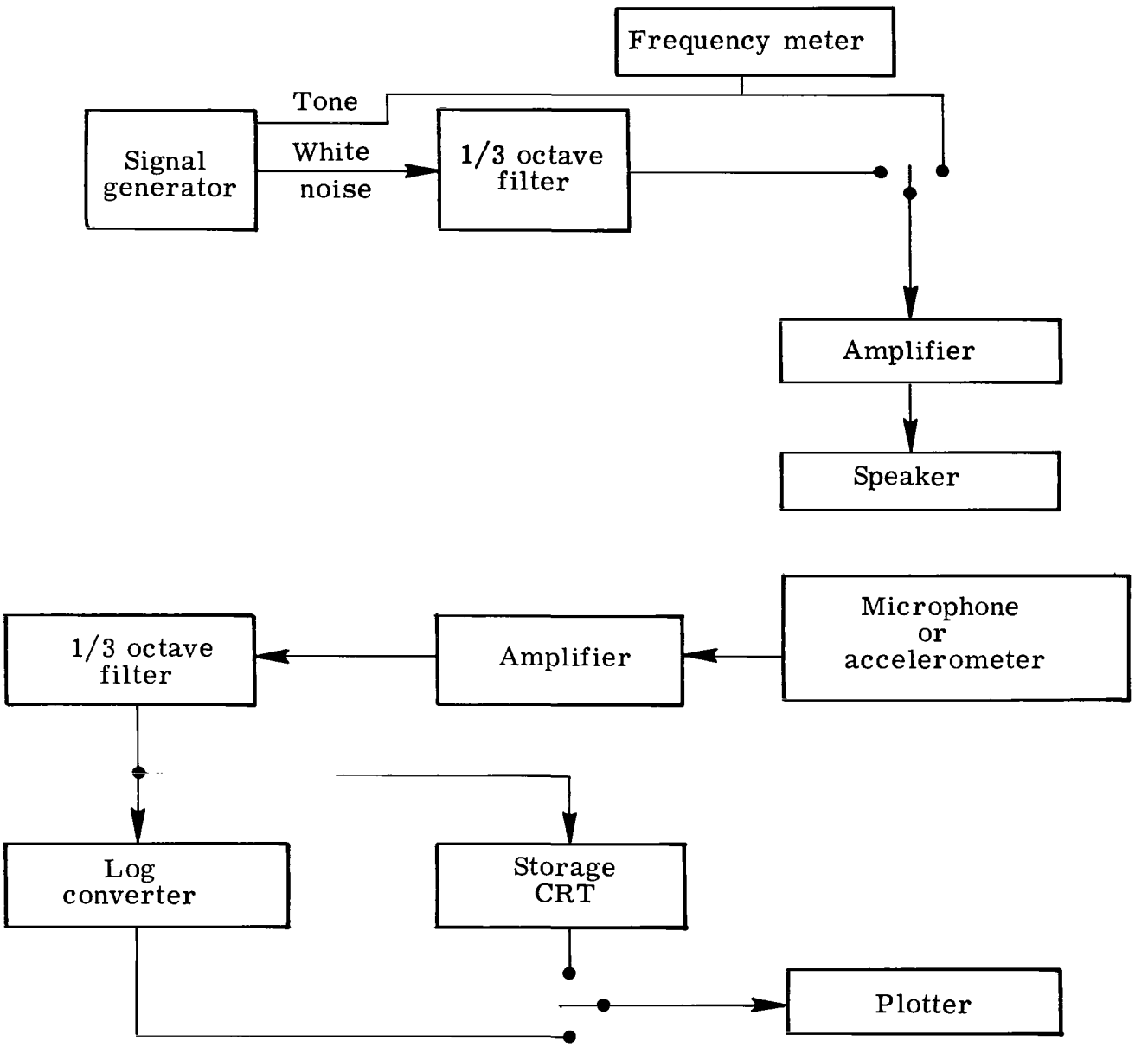

Figure 14.- Schematic diagram of instrumentation for measurement of reverberation time.

Calculated modes					
Mode m,n	Frequency, Hz	Mode m,n	Frequency, Hz	Mode m,n	Frequency, Hz
1,4	132	4,8	539	4,11	804
1,3	160	3,9	541	6,10	835
1,5	165	4,6	586	5,11	852
1,6	226	4,9	597	6,7	877
2,5	267	1,10	615	1,12	884
2,6	275	2,10	625	2,12	893
1,7	304	3,4	646	3,12	910
1,2	319	3,10	648	6,11	917
2,7	330	5,8	657	7,9	921
2,4	336	5,9	682	4,12	937
1,8	395	4,10	689	7,10	937
3,6	401	5,7	693	7,8	962
3,7	403	4,5	730	1,1	976
2,8	412	1,11	743	2,2	977
3,8	456	5,10	751	5,12	977
3,5	473	2,11	753	3,3	979
1,9	499	3,11	772	4,4	986
2,9	511	6,9	792	7,11	1 000
2,3	528	6,8	802	5,5	1 001
4,7	529	5,6	802	6,6	1 027

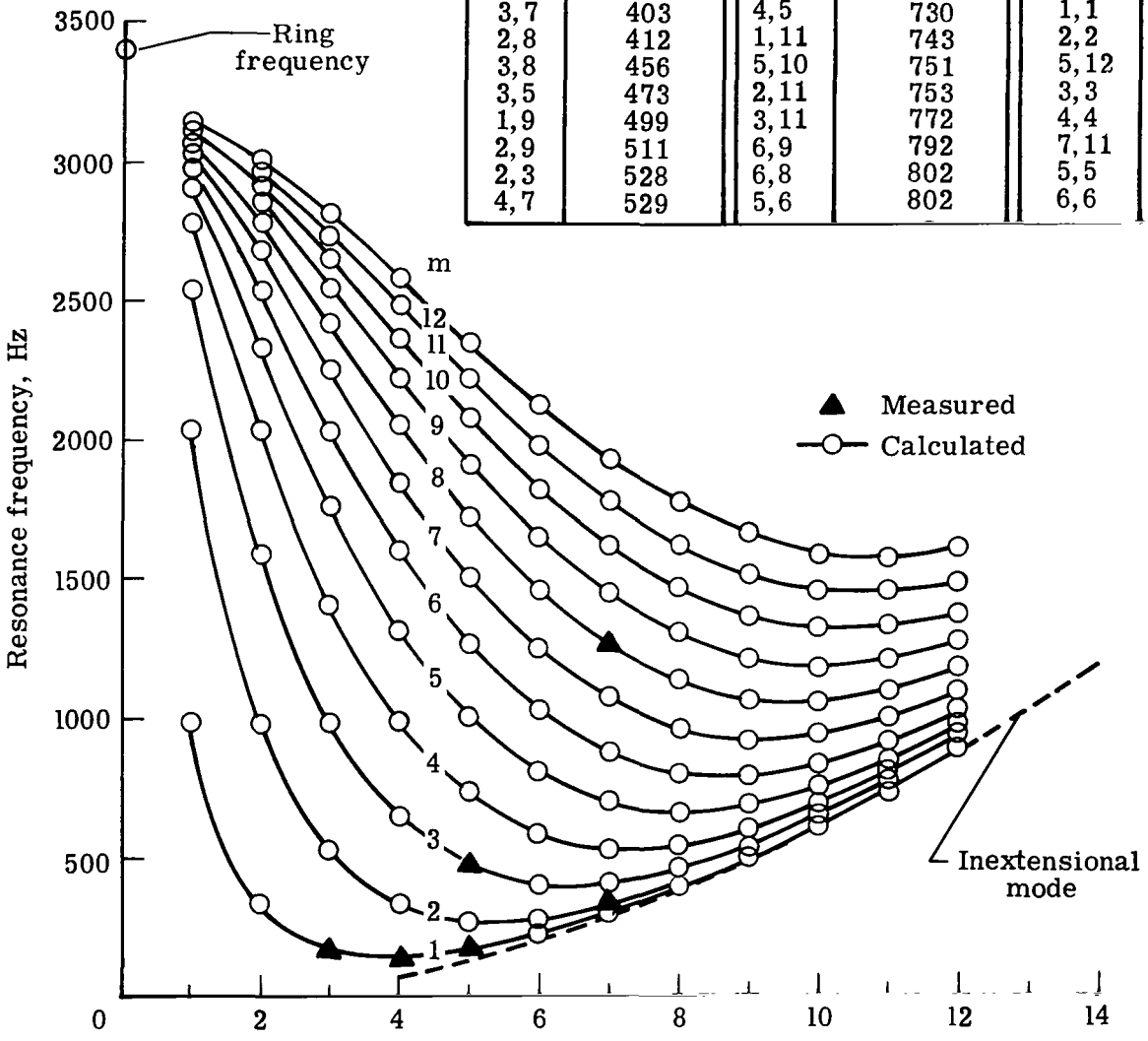

(a) Structural modes.

Figure 15.- Mode lattice for cylinder.

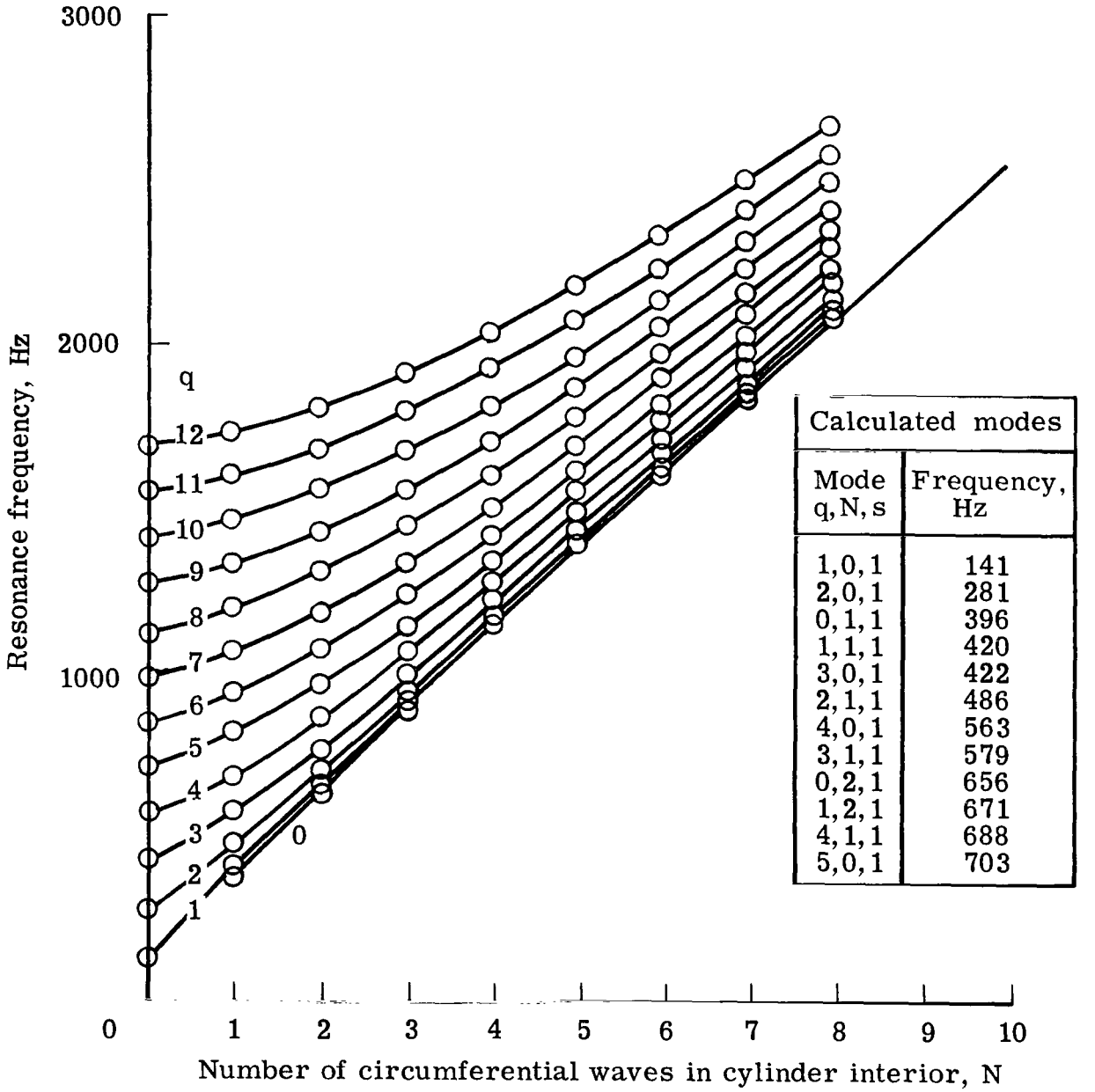

(b) Acoustic modes from reference 2. s = 1.

Figure 15.- Concluded.

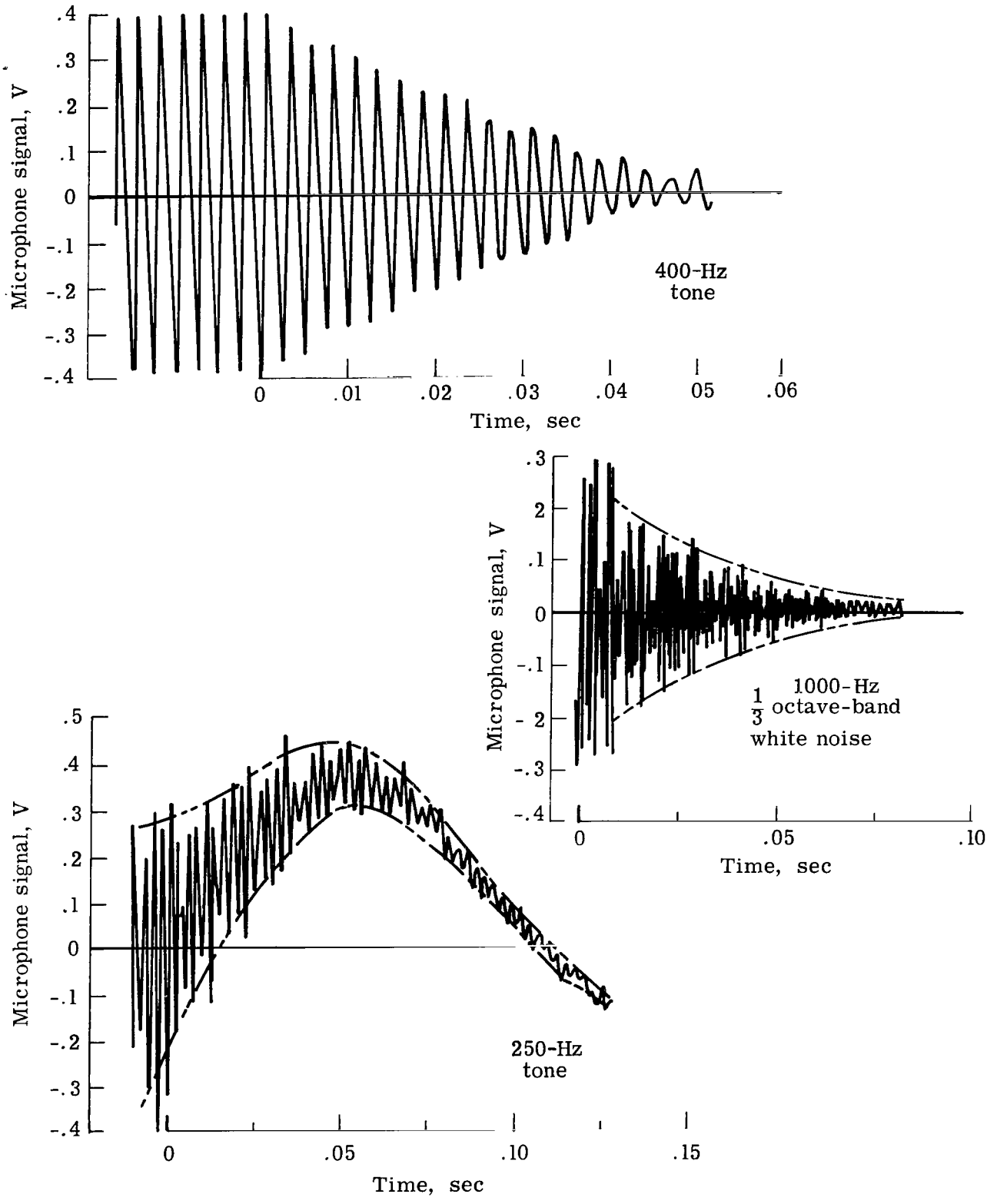

Figure 16.- Typical time histories of acoustic decay inside cylinder.

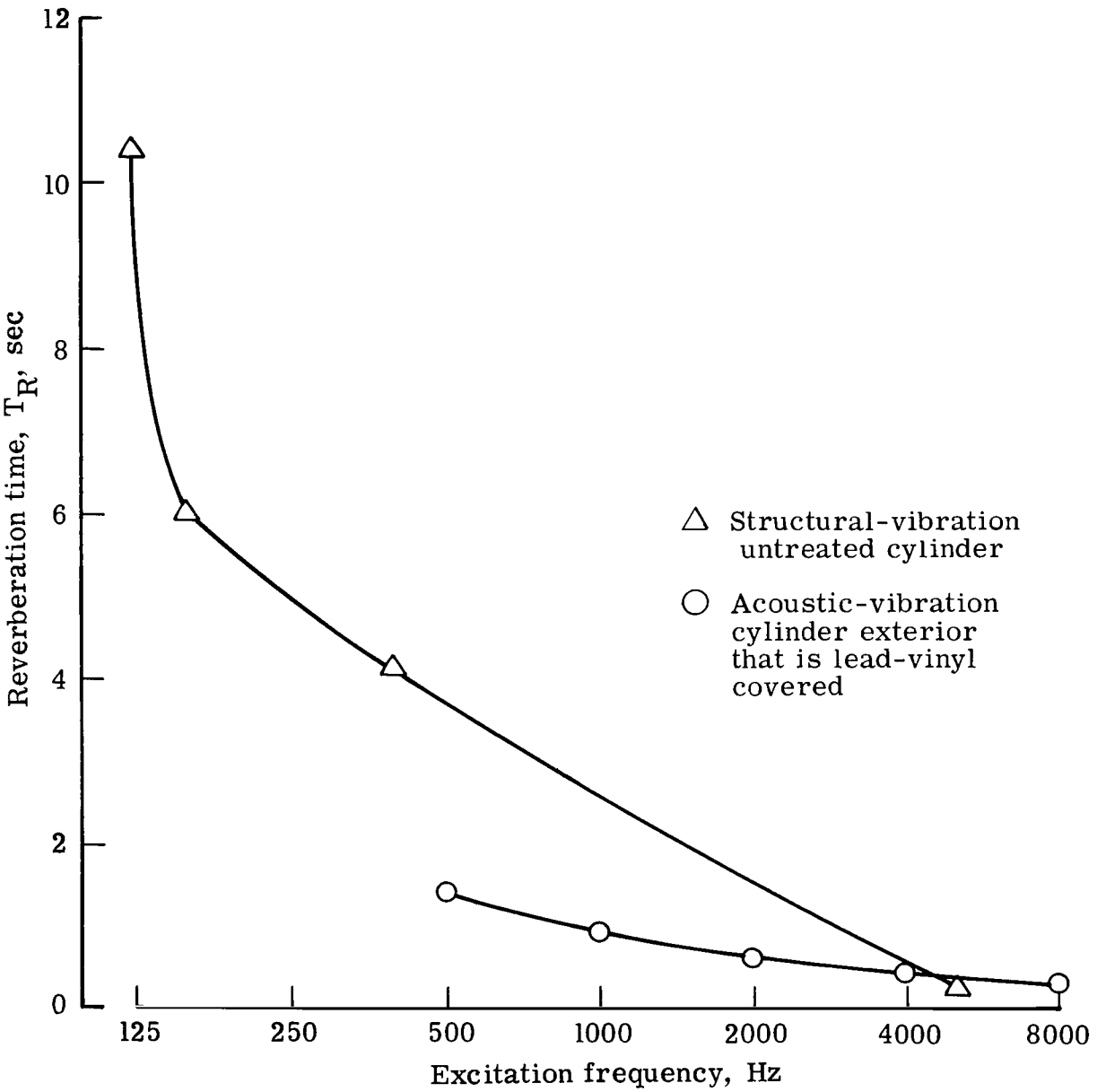

Figure 17.- Decay rates for acoustic and structural vibrations.

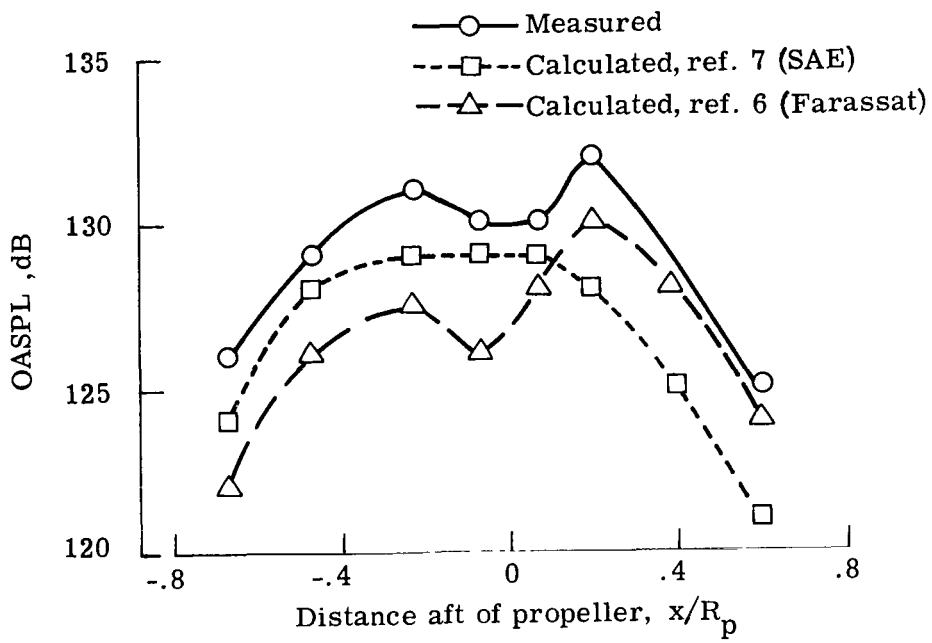

(a) Overall sound pressure level.

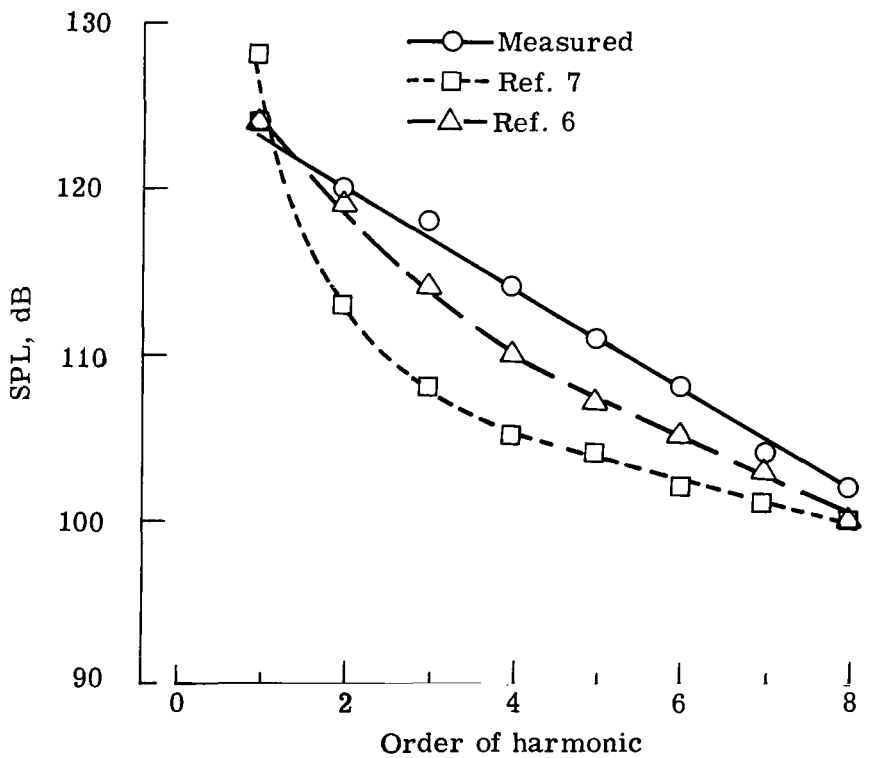

(b) Level of individual harmonics. $x/R_p = -0.07$.

Figure 18.- Comparison of measured and calculated SPL. 4000 rpm.

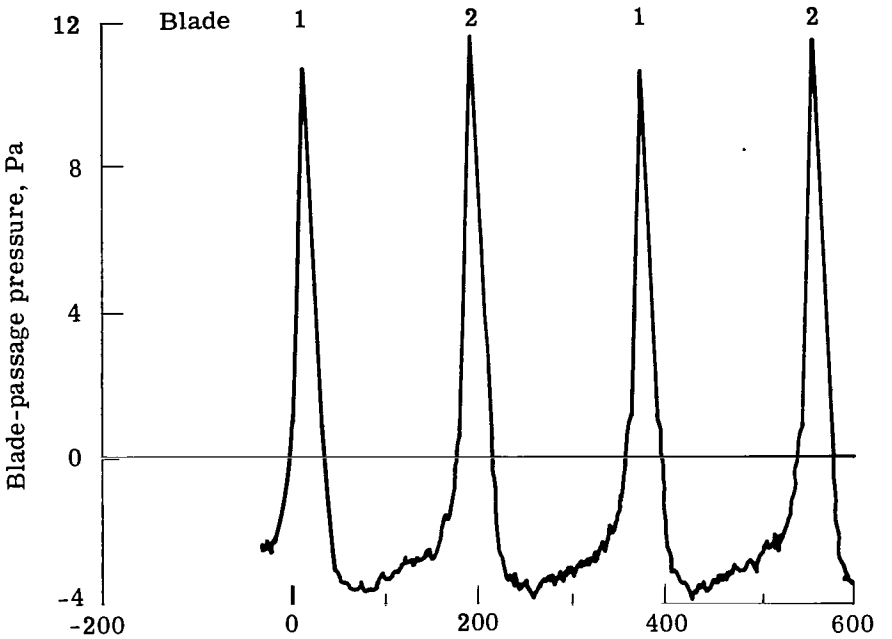

(a) $x/R_p = -0.07$.

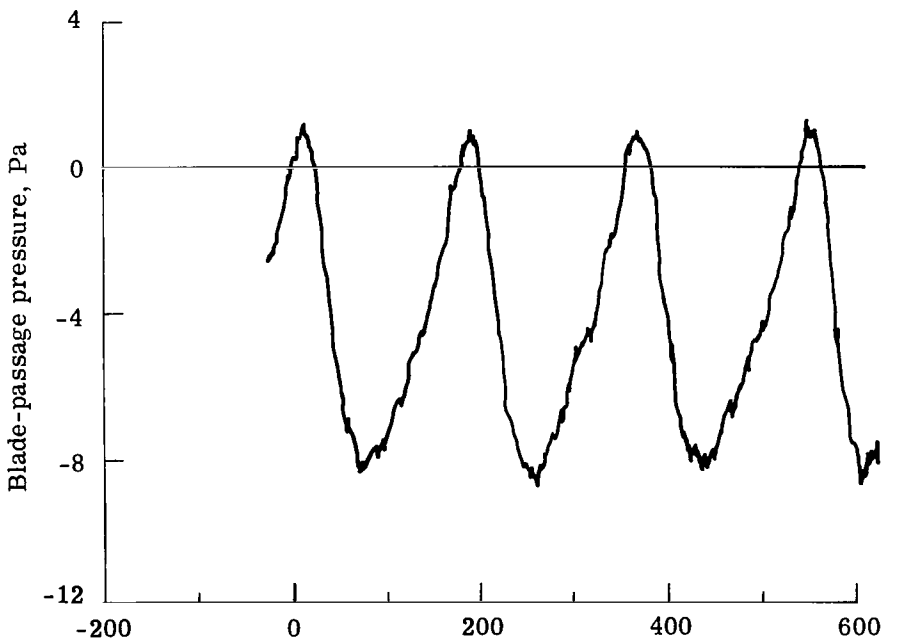

(b) $x/R_p = -0.67$.

Figure 19.- Time history of blade-passage pressure. 2000 rpm.

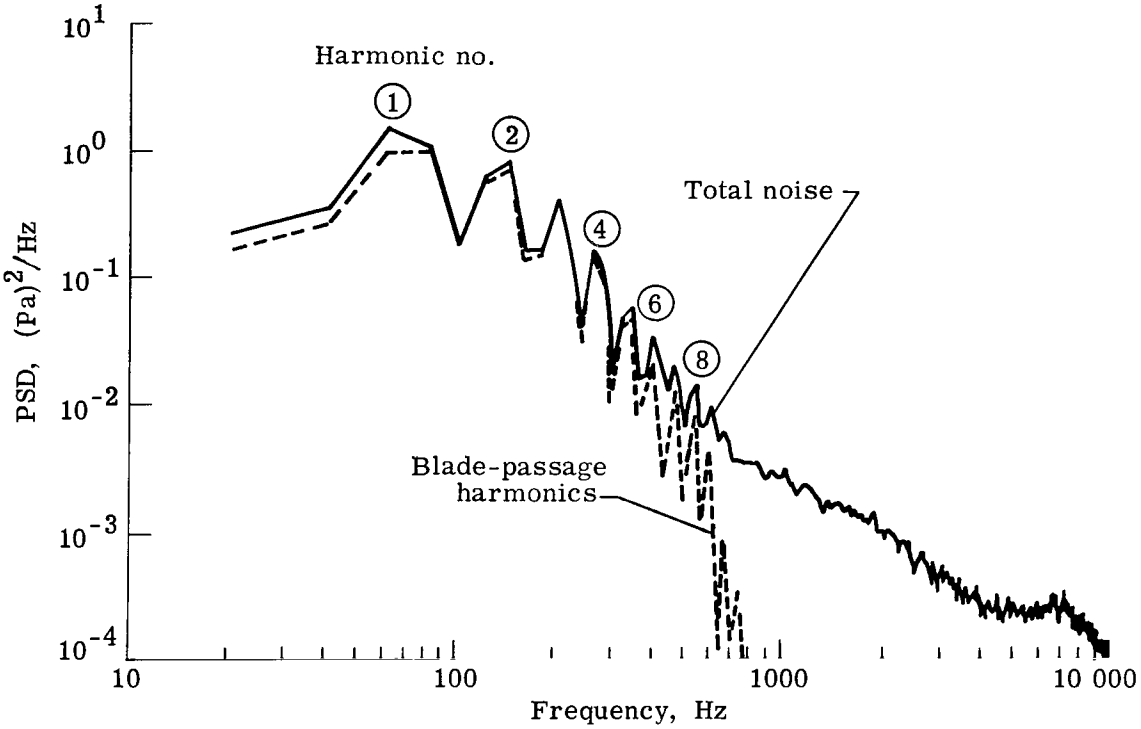

Figure 20.- Comparison of blade-passage noise with total noise. 2000 rpm; 20-Hz analysis bandwidth; $x/R_p = -0.07$.

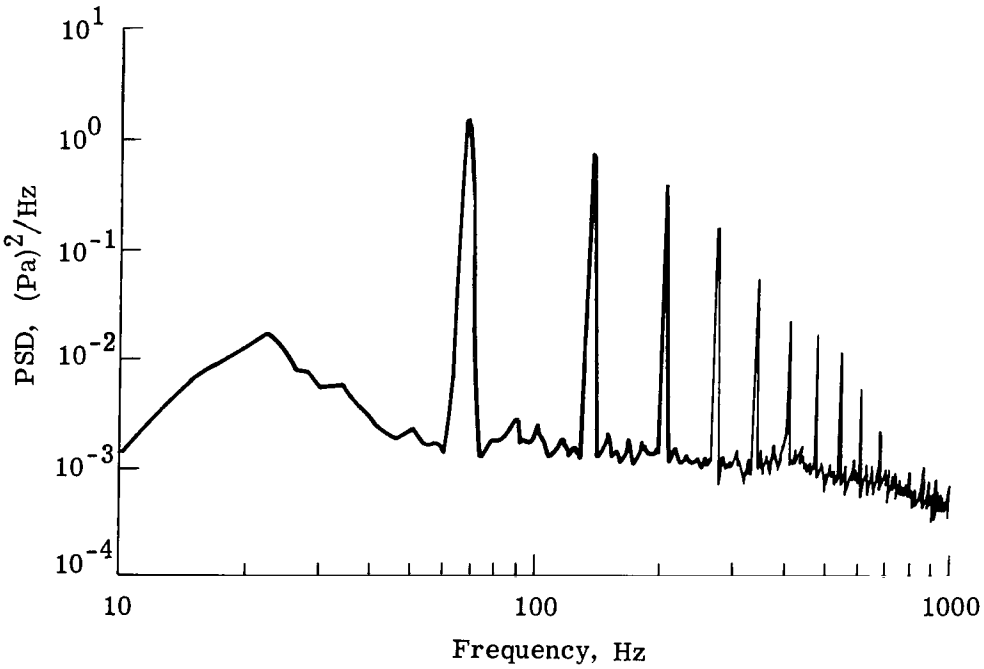

Figure 21.- Typical propeller-noise power spectral density. 2000 rpm; 2-Hz analysis bandwidth.

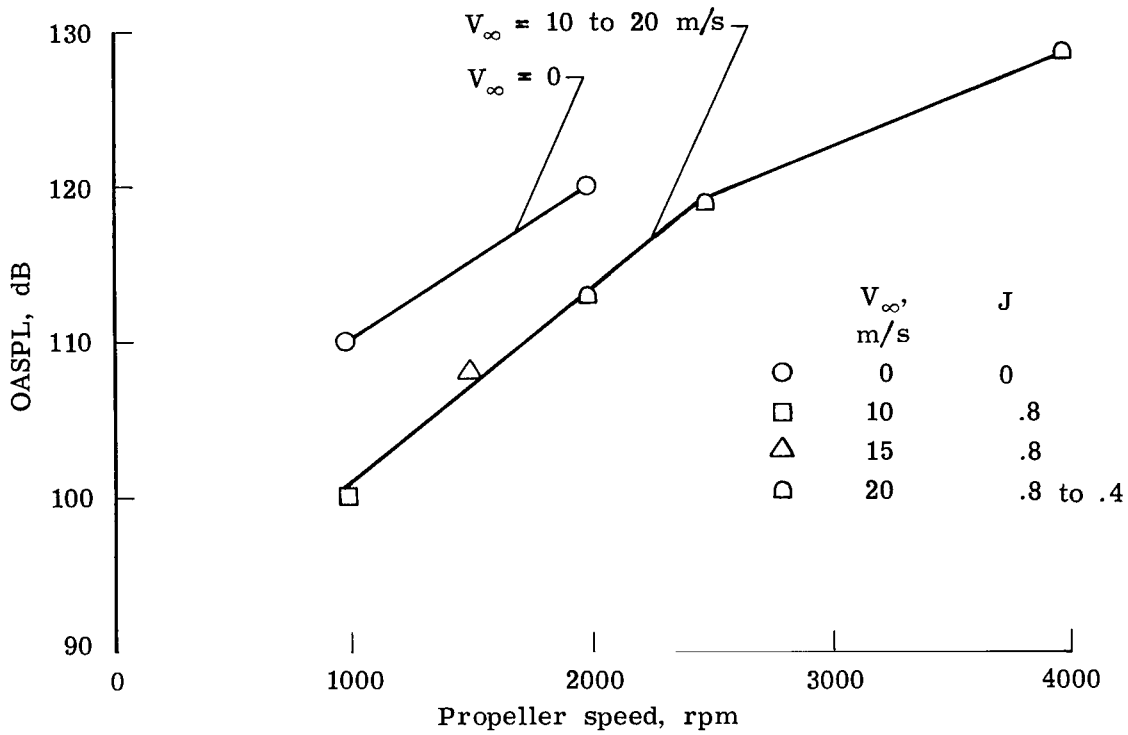

Figure 22.- Effects of forward velocity and propeller speed. $x/R_p = -0.07$.

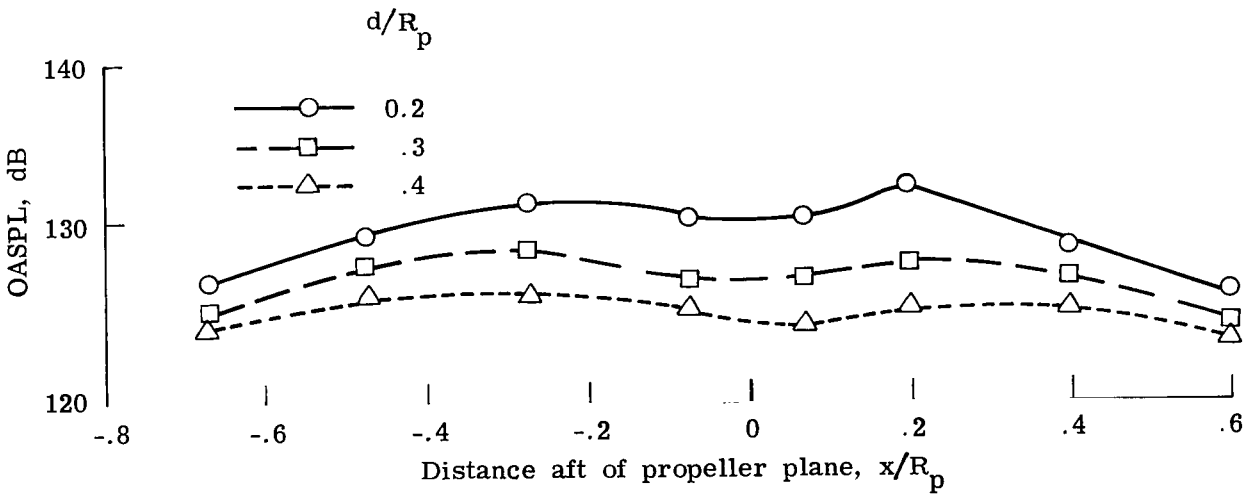

Figure 23.- Comparison of OASPL for three values of propeller tip clearance. 4000 rpm.

1. Report No.	2. Government Accession No.	3. Recipient's Catalog No.
NASA TP-1964		

4. Title and Subtitle
EXPERIMENTAL STUDY OF NOISE REDUCTION FOR AN UNSTIFFENED CYLINDRICAL MODEL OF AN AIRPLANE FUSELAGE

5. Report Date
December 1981

6. Performing Organization Code
505-33-53-03

7. Author(s)
Conrad M. Willis and Edward F. Daniels

8. Performing Organization Report No.
L-14878

9. Performing Organization Name and Address
NASA Langley Research Center
Hampton, VA 23665

10. Work Unit No.

11. Contract or Grant No.

12. Sponsoring Agency Name and Address
National Aeronautics and Space Administration
Washington, DC 20546

13. Type of Report and Period Covered
Technical Paper

14. Sponsoring Agency Code

15. Supplementary Notes

16. Abstract

Noise reduction measurements have been made for a simplified model of an airplane fuselage consisting of an unstiffened aluminum cylinder 0.5 m in diameter by 1.2 m long with a 1.6-mm-thick wall. Noise reduction was first measured with a reverberant-field pink-noise load on the cylinder exterior. Next, noise reduction was measured by using a propeller to provide a more realistic noise load on the cylinder. Structural resonance frequencies and acoustic reverberation times for the cylinder interior volume were also measured. Comparison of data from the relatively simple test using reverberant-field noise with data from the more complex propeller-noise tests indicates some similarity in both the overall noise reduction and the spectral distribution. However, all of the test parameters investigated (propeller speed, blade ptich, and tip clearance) had some effect on the noise-reduction spectra. Thus, the amount of noise reduction achieved appears to be somewhat dependent upon the spectral and spatial characteristics of the flight conditions. Information is also presented on cylinder resonance frequencies, damping, and characteristics of propeller-noise loads.

17. Key Words (Suggested by Author(s))	18. Distribution Statement
Interior noise Noise reduction Propeller noise	Unclassified - Unlimited Subject Category 71

19. Security Classif. (of this report)	20. Security Classif. (of this page)	21. No. of Pages	22. Price
Unclassified	Unclassified	34	A03

For sale by the National Technical Information Service, Springfield, Virginia 22161

NASA-Langley, 1981

National Aeronautics and
Space Administration

Washington, D.C.
20546

Official Business
Penalty for Private Use, $300

THIRD-CLASS BULK RATE

Postage and Fees Paid
National Aeronautics and
Space Administration
NASA-451

2 1 U,.1, 121481 5099305
DEPT OF THE AIR FORCE
AF WEAPONS LABORATORY
ATTN: TECHNICAL LIBRARY (SUL)
KIRTLAND AFB NM 87117

NASA

POSTMASTER: If Undeliverable (Section 158 Postal Manual) Do Not Return